Chapter 1
High-Resolution Electron Energy Loss Spectroscopy: Absolute Cross Section Measurements for Low Energy Electron Scattering from Biomolecules

V. Lemelin and L. Sanche

1.1 Introduction

1.1.1 General

The passage of high-energy particles or photons in biological matter produces copious numbers of secondary species along their tracks. It is well established that high-energy ionizing radiation (HEIR) deposits most of its energy in biological media via the secondary electrons it generates (Inokuti 1983; Pimblott et al. 1996; Boudaïffa et al. 2000; Pimblott and LaVerne 2007; Mucke et al. 2010; Duque et al. 2015). About 40,000 electrons per MeV of deposited energy (Pimblott and LaVerne 2007) are produced by single and multiple ionizations of biomolecules. Due to their abundance and their high reactivity, secondary electrons are considered as one of the most important species in radiobiology (Pimblott and LaVerne 2007; Mucke et al. 2010). The vast majority of these electrons have energies of less than 30 eV (Pimblott et al. 1996), the most probable energy being 9–10 eV (Pimblott and LaVerne 2007). These low-energy electrons (LEEs) interact with biological media by inelastic processes to vibrationally or electronically excite or ionize biomolecules. Subsequently, LEEs either recombine with ions or are thermalized by multiple processes such as intermolecular trapping, solvation, dissociative electron attachment (DEA) or resonance stabilisation. Ion-electron recombination and LEE inelastic scattering can create highly-reactive species including excited molecules, cations, anions and radicals. These species can damage cell components, change the biochemistry of the cell and create DNA damage. If DNA lesions are not repaired, they can lead to mutage-

V. Lemelin · L. Sanche (✉)
Department of Nuclear Medicine and Radiobiology, Faculty of Medicine and Health Sciences, Université de Sherbrooke, 3001 12e Avenue Nord, Sherbrooke, QC, Canada
e-mail: leon.sanche@usherbrooke.ca

V. Lemelin
e-mail: vincent.lemelin@usherbrooke.ca

A. S. Pereira et al. (eds.), *Radiation in Bioanalysis*, Bioanalysis 8,
https://doi.org/10.1007/978-3-030-28247-9_1

nesis and lethality (Chiari et al. 2014). Moreover, it has been shown that LEEs even of sub-ionization energies can induce cluster DNA damage (Boudaïffa et al. 2000; Huels et al. 2003; Chen et al. 2016; Shao et al. 2017) and thus have the capacity to induce cell death.

The primary objective of radiobiology is a complete understanding of the biological effects of HEIR. Since LEEs are one of the most abundant immediate species formed following irradiation, it is necessary to comprehend and model their interactions within biological media. Radiobiological models often rely on Monte Carlo (MC) simulations that can describe event-by-event modifications of the biological medium, predict the number of secondary species created and calculate the deposited energy after the passage of HEIR (Muñoz et al. 2008; Alloni et al. 2012; Liljequist et al. 2012; Sanz et al. 2012). These MC and track-structure calculations require a large number of parameters and values that are related to interaction probabilities, including cross sections (CSs). Because of the abundance and strong interactions of LEEs, MC simulations should incorporate as many CSs for their interactions with biological matter as possible (i.e., vibrational and electronic excitations, ionization, elastic scattering, DEA, etc.), to most accurately represent the biological effects of HEIR. Since biological media typically exist in a condensed phase, such CSs should be preferably measured in this phase.

In this chapter, we explain the use of high-resolution electron energy loss spectroscopy (HREELS), as a powerful experimental technique to study and measure absolute CSs for LEEs scattering from condensed molecules. We provide data on absolute CSs from the literature, which were derived from HREELS experiments with biologically relevant molecules, including those of the basic DNA constituents (Fig. 1.1). Even though this chapter is focused on CSs for dose calculations, particularly in localized radiotherapy, these values for LEEs induced processes are relevant to many other fields in which HEIR, and hence LEEs, play important roles. These include astrochemistry (Kaiser 2002; Holtom et al. 2005; Lafosse et al. 2006; Bennett and Kaiser 2007; Esmaili et al. 2017, 2018), planetary science (Lu and Sanche 2001; Samara et al. 2015), high-energy electron and extreme UV photon nanolithography (Wu et al. 2010), dosimetry for irradiation in space (Sridharan et al. 2015), plasma science (Lozano et al. 2017), biomedical imaging (Brix et al. 2005; Einstein et al. 2007; Eisenberg et al. 2011; Fazel et al. 2016) and radioprotection (Siragusa et al. 2017).

1.1.2 Radiotherapy Modalities and Low-Energy Electrons

The most important parameter to predict in any radiotherapy treatment is the energy deposited by HEIR per unit mass (i.e., absorbed dose (J/kg or Gy)). This parameter is crucial to maximise the damaging effects of HEIR to cancer cells, while minimizing them for healthy cells (Gaze 1996; Connell and Hellman 2009). Conventional radiotherapy modalities (e.g., external irradiation) deposit doses in macroscopic volumes (i.e., at organ and tissue level (>mm^3)). Radiobiological models presently used for

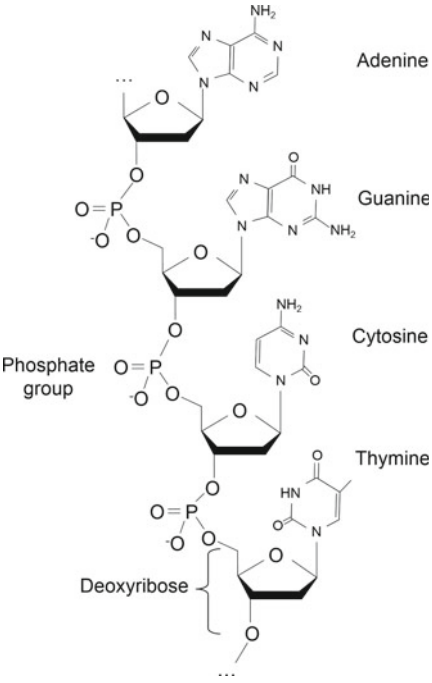

Fig. 1.1 Chemical structure of a short DNA strand including its four bases (Adapted from Lemelin et al. (2017), with the permission of AIP Publishing.)

these conventional treatments accurately predict the macroscopic doses (i.e., macro-dosimetry) to be administrated to patients. In conventional radiotherapy modalities, healthy cells are inevitably exposed to HEIR, thus increasing the risk of their death or of later secondary cancer development (Hall and Wuu 2003). It is thus crucial to protect healthy cells from HEIR. Moreover, macro-dosimetric methods usually take into account only the primary particles (high-energy photons and particles) and their interactions with molecules of the biological media, particularly the water molecules (Meesungnoen et al. 2002; Emfietzoglou et al. 2005; Plante and Cucinotta 2009; Francis et al. 2011). Hence, while they can calculate the macroscopic dose, they do not consider the damage produced at the cellular and molecular levels by LEEs and other reactive species.

New radiotherapy modalities are being developed to selectively deliver a toxic dose exclusively to cancer cells, while preserving healthy cells (Gaze 1996; Seiwert et al. 2007; Reilly 2008; Connell and Hellman 2009; Chattopadhyay et al. 2010; Zalustky 2013; Sanche 2015; Hayes 2017; Rezaee et al. 2017). These new modalities focus on delivering localized nanoscopic or molecular doses using the reactivity of LEEs and/or other secondary species (Rezaee et al. 2017). Targeted radionuclide therapy (TRT) (Chattopadhyay et al. 2010; Hayes 2017) and concomitant chemoradiation therapy (CRT) (Seiwert et al. 2007) are two examples of these new improved modalities. The former uses radio-labeled molecules that localize preferentially in cancer cells and release, for example, Auger electrons (Zalustky 2013). Since the energy distribution of Auger electrons lies at low energy, they have short range

(~10–12 nm) and generate a large quantity of secondary LEEs in the vicinity of the cancer cell. These LEEs thus have the capacity to deposit most of their energy at the DNA level. Furthermore, the density of LEEs can be increased by combining targeted radionuclides with gold nanoparticles (GNPs) or by embedding radionuclides in gold nanocages (Sanche 2015). In these cases, the longer-range particles or photons emitted by the radionuclide strongly interact with the heavy metal, generating large quantities of LEEs. The incorporation of GNPs in TRT is an active field of research (Reilly 2008; Chattopadhyay et al. 2010; Hainfeld et al. 2010; Rezaee et al. 2017; Ghandi et al. 2018) and considerable efforts are being made to improve this new modality. Multiple studies (Hainfeld et al. 2004, 2008, 2010; Hyun Cho et al. 2005; Kong et al. 2008; Rahman et al. 2009; Lechtman et al. 2011; Chattopadhyay et al. 2013) have demonstrated dose and damage enhancements by GNPs in biological tissues, marking them promising tools for future radiotherapeutic treatments.

In cancer therapy, clinical protocols often combine chemotherapy, surgery and radiotherapy. CRT is the combination of chemotherapeutic agents (CAs) and radiotherapy, an approach that often enhances tumor treatment (Seiwert et al. 2007) since, when used in concomitance with HEIR, CAs can often radiosensitize cancer cells. It has been shown that CRT may rely, at least in part, on an increase in damage inflicted to the genome of the cancer cells due to the binding of the CA to DNA.

Conventional methods of estimating radiation doses for macroscopic volumes are obviously not suitable for predicting the subcellular radiobiological effectiveness of these new modalities. TRT and CRT require the details of energy deposition at the nanoscopic level to predict damages and radiobiological risks associated with locally delivered doses. Since these rely on the damages induced by secondary particles such as LEEs, TRT and CRT require new dosimetric models that can predict and calculate doses and damages at subcellular levels. Therefore, it is imperative to develop and improve nanodosimetric models for the continued development of these promising targeted radiotherapy modalities.

1.1.3 Monte Carlo Simulations and Nanodosimetry

MC simulations can predict damage to a biological medium and the deposited dose at nanoscopic scales, produced by primaries and secondary species, including LEEs (Rogers 2006; Nikjoo et al. 2016). Thus, TRT and CRT can benefit from the detailed description that MC simulations provide. However, for accuracy, MC codes must incorporate a panoply of CSs values for LEE interactions with the biological medium. MC simulations in water have received the most attention (Meesungnoen et al. 2002; Emfietzoglou et al. 2005; Plante and Cucinotta 2009; Francis et al. 2011) and CSs for LEEs interactions with water are incorporated in MC codes, such as Geant4-DNA simulation toolkit (Kyriakou et al. 2017), PENELOPE (Kyriakou et al. 2017) and TOPAS-nBio (McNamara et al. 2017). The general conclusion from these studies is that in MC simulations, LEEs interactions with water and biological medium play a

crucial role in describing the chemical and biophysical stages of radiation damage in cells.

Many parameters are user-defined in MC simulations, particularly in modelling radiation damage to DNA (Pater et al. 2014). For each relevant biomolecule present in cells and their nuclei, (e.g., water, DNA fundamentals units, amino acids, etc.), the various parameters needed for MC simulations include CSs for: total ionization, total excitation, total elastic scattering, partial ionization, electronic and vibrational excitation and phonon scattering of all particles involved in the energy deposition process. More specifically, MC simulations require such integral and differential CSs for all the relevant interaction mechanisms involving the fundamental units of DNA. Presently, there is a lack of information on these CSs for material relevant to radiation biology. There exist various experimental techniques to probe LEE-induced processes in biomolecules, including DNA, and measure corresponding CSs; these include X-ray photoelectron spectroscopy (XPS) (Klyachko et al. 1999), electron stimulated desorption (ESD) (Hervé Du Penhoat et al. 2001), electron transmission spectroscopy (ETS) (Burrow et al. 2008), coupled with chemical analysis of degradation products.

The next section focuses on HREELS, one of the most powerful tools to generate CSs for LEE-scattering from biomolecules. We will explain from basic principles, how this is possible and provide the most complete set of absolute CSs for condensed DNA constituents available.

1.2 Absolute Cross Sections Measurements with HREELS

1.2.1 Condensed Phase Scattering

At sufficiently high energy, the electron's wavelength is usually much smaller than the distance between biomolecules in cells. Accordingly, above about 100 eV, electrons interactions may begin to be approximated by collisions with individual targets for fairly disordered materials. Below this energy, the wavelength of a LEE may be comparable to intermolecular and interatomic distances, hence permitting simultaneous interactions with multiple targets (Bauer 1994). In fact, various quantum phenomena appear at low energies, such as diffraction of the electron's wave by the molecules of the solid (Zheng et al. 2006) and effects from the band structure of the molecular solid (Nagesha and Sanche 1998). Also, in condensed media, many excitation modes can be affected and new modes such as intermolecular vibrations or phonons are observed (Michaud et al. 2003). To take into account these latter processes and quantum phenomena, as well as to study biomolecules as close as possible to their biological environment, CSs should be preferably measured in condensed phase. This chapter focuses on the generation of absolute LEE-scattering CSs from off-specular HREELS data.

1.2.2 HREEL Spectroscopy

HREEL spectroscopy has been widely applied to many areas of surface and interface related research, e.g., to characterize substrates and adsorbates on surfaces. Multiple review articles exist on this technique (Ibach and Mills 1982; Bass and Sanche 1998; Lafosse and Azria 2011; Conrad and Kordesch 2017). As shown in this section, HREELS can also produce electron-scattering CSs for both gas and condensed phase molecules. For the latter, the majority of studies have focused on DNA constituents, such as the molecular moieties of its backbone (i.e., deoxyribose and phosphate group) and the bases (i.e., adenine, cytosine, thymine and guanine), as well as self-assembled monolayers (SAM) of DNA (Vilar et al. 2008).

Figure 1.2 represents a schematic diagram of a typical HREEL spectrometer for condensed-phase measurements. It consists of two hemispherical electrostatic deflectors; a monochromator and an analyzer (Michaud and Sanche 1984a). The monochromator produces monoenergetic electrons with energy ranging from 0 to 100 eV. In some HREELS systems, the monochromator and the analyzer can be rotated around the target. In this manner, it is possible to study the angular depen-

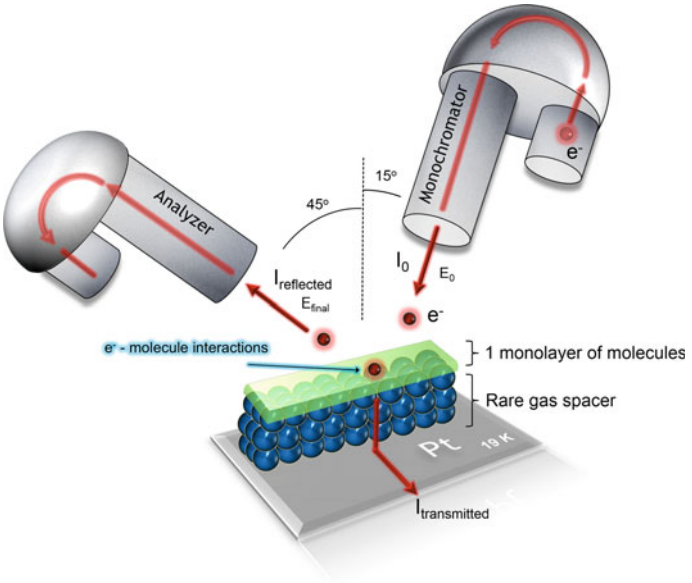

Fig. 1.2 Schematic representation of a High-Resolution Electron Energy Loss Spectrometer (HREELS) and solid phase target. The arrangement is composed of two electrostatic hemispheres: a monochromator and an analyzer. In this setup, monoenergetic electrons produced by the monochromator are incident at 15° from the normal of a platinum substrate surface, which is covered by a rare gas spacer layer held at 19 K. Biomolecules are condensed on the spacer layer. The analyzer measures the intensity of electrons inelastically scattered at 45° in the opposite azimuth. The total electron current transmitted through these layers can also be measured

dence of the electron scattering process with the condensed biomolecules. All the components are housed in an ultra-high vacuum chamber (UHV) where biomolecular films may be prepared by cryogenic condensation, as thin molecular solids. In the majority of such experiments, a metal substrate is cooled to temperatures between 15 and 100 K. First an inert rare gas spacer of several monolayer thickness (ML) is condensed on the metal surface. Afterwards, a monolayer or sub-monolayer of the biomolecular target is deposited. Spacer films of inert rare gas (usually Ar or Kr) reduce molecule-metal substrate interactions and image-charge polarization (Michaud and Sanche 1994). In the case of Ar films, the inert nature and large band gap ensure that electron scattering within the spacer layer is essentially elastic (Levesque et al. 2005a, b; Michaud et al. 2012) below the energy threshold of exciton creation (11.75 eV). These cryogenic conditions are needed in order to supress the vibrational and phonon excitations of the molecular solid and the substrate, and to observe preferentially the interactions of electrons with molecules in their ground state. The resolution of the electron spectrometer can vary from 1 to 60 meV full width at half maximum (FWHM) depending on the incident current I_0, the incident and scattered angle (θ_0 and θ_d, respectively) and on the optimization of the working conditions of the two hemispherical electrostatic deflectors.

1.2.2.1 Excitation Mechanisms

There exist two main classes of electron scattering with a medium or molecules: direct and resonant scattering. Direct scattering is mainly controlled by the exchange force and permanent and induced electrostatic potentials. The permanent or induced dipolar term is often the major contribution in the expansion of these potentials. It arises from long-range Coulombic interactions that operate at electron-molecule distances of between ~10 and 100 Å (Lafosse and Azria 2011). Resonant scattering takes place on a much shorter range, at around ~1–3 Å (Lafosse and Azria 2011). Contributions from each of these mechanisms in HREEL spectroscopy depends considerably on the experimental conditions; the incident energy E_0, the incident (θ_0) and analyzing angle (θ_d). With dipolar scattering, the incident electron induces vibrational or electronic excitations via interaction with the dynamic dipole of the molecules or the solid. Since the electron interacts with a long-range Coulomb potential, it scatters with a small change in its wave vector ($\Delta k \ll k$) causing the electrons to scatter predominantly in the specular direction (Lafosse and Azria 2011). For the resonant mechanism, the vibrational or electronic excitations are induced via short-range interactions of the incoming electron with the atomic or molecular potential of the surface or near-surface components (Schulz 1976). With this type of interaction in a randomly oriented molecular film, the LEE wave vector experiences large momentum changes, with no particular backscattered direction being favored. Since dipolar (i.e., optical) selection rules no longer prevail in resonance scattering, multiple excitation losses are enhanced relative to dipolar scattering and electron resonances can be observed. These consist in the temporary capture of the incoming electron by a previously empty atomic or molecular orbital (Sanche and Schulz 1972) to form

a transient negative ion (TNI). There exist mainly two types of resonances: shape and core-excited resonance (Sanche and Schulz 1972; Schulz 1973). The shape or single particle resonance occurs usually at low energies (0–5 eV), when the incoming electron occupies a previously empty orbital of the molecule in its ground state (Caron and Sanche 2011). It is called "shape" resonance, because the electron is captured by the shape of the effective potential barrier created by the electron and the molecule (Schulz 1973). In a core-excited resonance, the capture of the incoming electron involves also electronic excitation of the target molecule (Schulz 1973). A core-excited resonance is also called a "two-electrons one-hole state", since it involves the movement of an electron from a lower energy orbital to a higher one. In either type of resonances, the TNI is formed at a specific energy corresponding to that of the anion's transient state involved. At resonance energies, CSs for electron interactions can be considerably enhanced.

During the life-time of the TNI, the nuclei may move apart from the equilibrium position due to the perturbation induced by the extra electron (Arumainayagam et al. 2010). The TNI has multiple outcomes or decay channels. In the autodetachment channel, this perturbation can result in a vibrationally excited neutral molecule (Arumainayagam et al. 2010). If the TNI is sufficiently long-lived and its inter-atomic potential energy surface is repulsive, the nuclei may move apart sufficiently for fragmentation of the anion, a process known as DEA, in which the electron is captured permanently by one fragment ($AB + e^- \rightarrow AB^- \rightarrow A^- + B$) (Sanche 2010).

TNIs are of considerable interest in radiobiology, since multiple studies have shown that the decay of these resonances can cause fragmentation of biomolecules including lethal DNA damages, particularly local multiply-damage sites (Boudaïffa et al. 2000; Sanche 2010; Chen et al. 2016; Shao et al. 2017). Thus, resonance scattering is probably one of the most relevant physical mechanisms to investigate in radiobiology.

1.2.2.2 Condensed-Phase HREELS and Scattering Models

In its condensed-phase version, HREELS allows the study of elastic scattering and energy losses by electrons scattered inside or at the surface of a solid. There exist principally two modes of measurement. It is possible to measure the magnitude of a given energy loss by sweeping the energy of both the monochromator and the analyzer, while maintaining a constant potential difference between them corresponding to the probed energy loss (Michaud et al. 1991; Lepage et al. 1998). The recorded current is termed an excitation function for the given energy-loss process (e.g., a vibration or an electronic mode). Excitation functions provide information on the energy dependence of interaction probabilities (Lepage et al. 1998), which are required to detect the presence of TNI at certain incident energies, but reliable absolute CSs cannot be extracted from such measurements (Allan 2007).

In the electron energy loss (EEL) modes of HREELS, spectra are recorded by sweeping the potential of the analyzer relative to the grounded target and keeping constant the potential of the monochromator or vice versa. When the incident electron

energy (E_0) is kept constant, the analyzer measures electrons that have experienced a range of energy losses. Absolute CSs are usually measured in this mode. An example of a vibrational HREEL spectrum is shown in Fig. 1.3.

The sample molecules can be condensed as a multilayer film or isolated on a rare gas spacer. To condense molecules on the substrate, there exist two alternative methods, which depend on the phase of the sample at ambient temperature (T) and pressure (P). For samples that are gases or liquids under ambient conditions, the vapor is introduced into a gas-handling manifold (Michaud and Sanche 1984a). Thereafter, a controlled quantity of vapor, determined by a pressure change in the manifold can be expanded into the UHV chamber and condensed onto a substrate. Alternatively, for samples that are solid at ambient temperature and pressure, a double-stage oven has been developed by Lévesque et al. (2003) for film deposition. In a secondary chamber, a crucible containing the sample in powder form, is heated up to the point of sublimation. Sublimated molecules escape the crucible via an aperture and condense upon a ceramic tip that is positioned beside the crucible. Thereafter, the tip is brought into the UHV analysis chamber and positioned in front of the metal surface, at a distance of 5 mm. The tip is then heated to desorb the molecules, which condense onto the cooled substrate (Levesque et al. 2003).

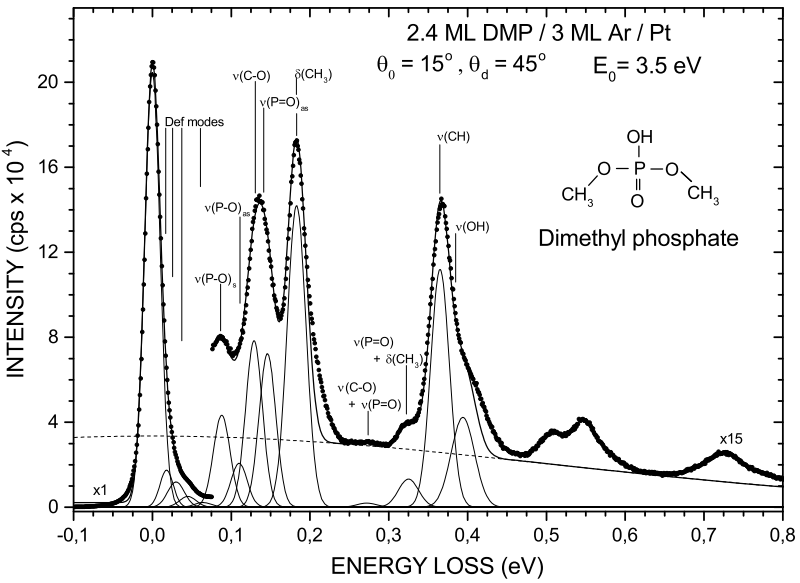

Fig. 1.3 A representative electron-energy-loss (EEL) spectrum recorded with 3.5-eV incident electrons on 2.4 monolayers (ML) of Dimethyl Phosphate (DMP) deposited on 3 ML of Ar. The thin solid line passing through the data points corresponds to the sum of Gaussian functions appearing at the bottom, which are associated with each vibrational peak. The dashed line accounts for the background current produced by the Ar and Pt substrates (Reproduced from Lemelin et al. (2017), with the permission of AIP Publishing.)

For extracting absolute CSs from LEE scattering data, two models have been developed to analyze results from either multilayer or (sub-) monolayer films. Dependent on film thickness, HREEL data are analyzed by a multiple scattering model (Michaud and Sanche 1987a; Michaud et al. 2003) or a single collision model (Levesque et al. 2005b; Bazin et al. 2010). In the latter, the elastically scattered current measured by the analyzer at an angle of θ_d, with respect to the surface normal, is assumed to have a diffuse reflectivity. Since this model only considers single collisions within a monolayer or submonolayer film, it can be shown that for an incident electron beam current I_0 of energy E_0, with a near normal incidence θ_0, the analyzer measures in the backscattered direction θ_d, a current of electrons with an energy E that have experienced an energy loss of $E - E_0$ into the film such that (Levesque et al. 2005b; Michaud et al. 2012):

$$I(\theta_d, E_0, E - E_0) \cong \frac{I_0(\theta_d, E_0)}{cos\theta_0}\sigma_r(E_0, E - E_0)n_s \tag{1.1}$$

where $\sigma_r(E_0, E - E_0)$ is the CS for an electron of energy E_0 to deposit an energy $E\text{-}E_0$ in the film and be backscattered into the vacuum; n_s is the surface number density of the target molecules (related to the thickness of the film). The term $I_0(\theta_d, E_0)$ is defined as an effective incident electron current and can be considered as that fraction of the total incident electron current I_0 that would be backscattered in the direction of the analyzer at θ_d by a material with a diffuse elastic reflectivity of one. This latter experimental parameter allows the normalization of EEL spectra and permits the energy integral over an energy loss feature to be expressed in terms of an absolute reflectivity value (Levesque et al. 2005b). To determine this value experimentally, a technique, which uses the linear relationship between the reflected and transmitted current has been developed and is described in detail elsewhere (Levesque et al. 2005b; Michaud et al. 2012). Briefly, the value of $I_0(\theta_d, E_0)$ can be determined from the conversion law between the backscattered and transmitted current (Levesque et al. 2005b; Michaud et al. 2012) and by extrapolation to zero thickness from measurements taken over a range of film thicknesses. Hence, from n_s and $I_0(\theta_d, E_0)$ values, it is possible to normalize EEL spectra ($I(\theta_d, E_0, E - E_0)$) and extract integral CSs for inelastically scattered electrons. To determine the absolute CS values, multiple EEL spectra $I(\theta_d, E_0, E - E_0)$ are recorded at different E_0. Subsequently, each energy-loss spectrum is fitted with multiple Gaussian functions to delimit the various excitation energy regions (vibrational and electronic excitations) (Levesque et al. 2005b; Michaud et al. 2012) as is illustrated in the representative EEL spectrum of Fig. 1.3 (the solid black line represents the fit from the sum of the Gaussians). Then, the absolute CS value $\sigma_{ri}(E_0, E - E_0)$, for a given excitation, is calculated using the area under the corresponding Gaussian function *i* with the amplitude of $a_i(E_0)$ and δ_i FWHM using:

$$\sigma_{ri}(E_0) = \frac{a_i(E_0)\delta_i\pi^{\frac{1}{2}}}{2(\ln 2)^{\frac{1}{2}}} \tag{1.2}$$

By varying E_0, it is possible to obtain the energy dependence of the absolute CSs for each excitation. The energy and the δ_i assigned to each Gaussian must stay constant between spectra and only the amplitude $a_i(E_0)$ can vary in order to produce each fit. It is important to note that the CSs extracted with the single collision model are integral and absolute values, if the backscattered intensity is isotropic and the electron only experiences single collisions; this is the case for the results that are presented starting in Sect. 1.2.3.2. Under near normal electron incidence and with azimuthally disordered film conditions (Levesque et al. 2003, 2005a, b), multiple studies (Michaud and Sanche 1984b, 1987b; Lepage et al. 2000) have shown that the backscattered intensity can be considered isotropic for the systems used in the studies discussed here. By measuring EEL spectra in a fixed direction and by normalizing to the effective current $I_0(\theta_d, E_0)$, the single collision model (Eq. (1.1)) leads to CS values corresponding to electrons backscattered over the whole half-angular space (Levesque et al. 2005b). Thereby, the CSs presented in this chapter are considered to be integral and absolute values.

1.2.3 Absolute Cross Sections for Condensed Biomolecules

1.2.3.1 Amorphous Ice

One of the most important and abundant molecules in cells and biological tissues, is water. CSs for LEE scattering by water molecules have therefore been measured in the condensed phase (Michaud and Sanche 1987a, b; Bader et al. 1988; Michaud et al. 2003) and the values implemented into MC simulations (Meesungnoen et al. 2003, 2015; Uehara and Nikjoo 2006; Dingfelder et al. 2009; Plante and Cucinotta 2009; Plante 2011; Francis et al. 2011, 2012; Plante et al. 2012; Douglass et al. 2015). We present and discuss in this section the results of Michaud et al. (Michaud and Sanche 1987a, b; Michaud et al. 2003). These authors generated absolute integral CSs for elastic collisions, phonon excitations, vibrational and electronic excitations and ionization, in the range 1–100 eV from analysis of HREEL data (Michaud and Sanche 1987a, b; Michaud et al. 2003). The absolute inelastic scattering CSs for incident electrons below 30 eV lie within the range of 5.6–9.8 $\times$ 10^{-17} cm^2 (Michaud and Sanche 1987a, b; Bader et al. 1988; Michaud et al. 2003). Since the electrons were incident on 30-ML films of water, a multiple-scattering analysis in a two-stream approximation was required to extract the CSs. The method is described by Michaud and Sanche (Michaud and Sanche 1987a). The energy-dependence of the elastic CS in the range 1–100 eV exhibits three broad structures at around 6.5, 14.5 and 40 eV as well as a small shoulder near 80 eV, as seen in Fig. 1.4a). These authors also measured the CSs for the translational phonon mode $\nu_{T''}$, the energy dependence of which exhibits a strong rise at low energy similar to the elastic CSs. The librational modes $\nu_{L'}$ and $\nu_{L''}$ have also been resolved and the 0–100 eV dependence of their CSs shows a rise at low energy (Fig. 1.4a)). Maxima around 8.5 and 7 eV are also observed for $\nu_{L'}$ and $\nu_{L''}$ respectively. At higher incident energy, librational CSs exhibit an oscillatory

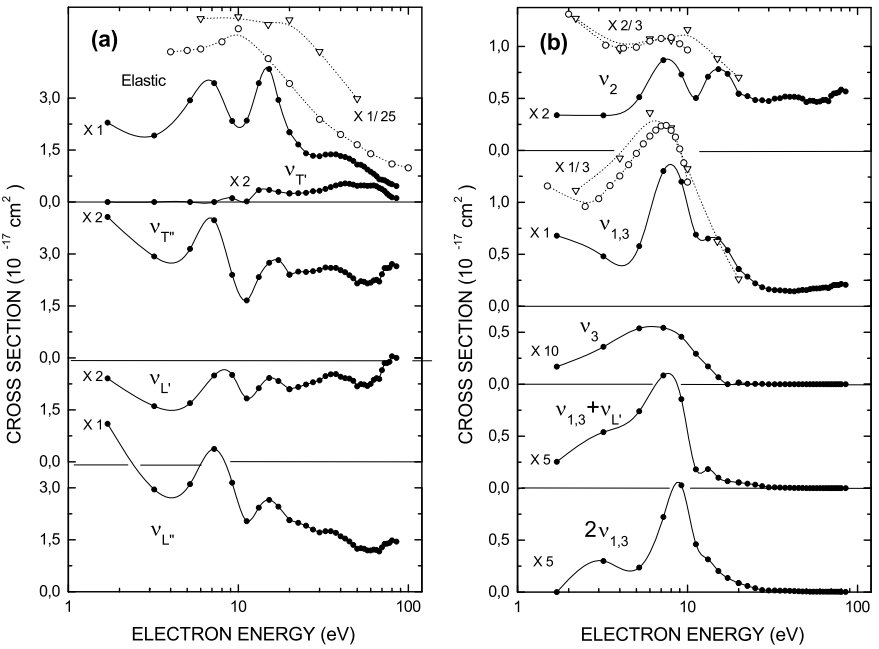

Fig. 1.4 Integral cross sections for **a** elastic scattering, translational ($\nu_{T'}$ and $\nu_{T''}$) and librational phonons modes ($\nu_{L'}$ and $\nu_{L''}$) and **b** vibrational modes ν_2, $\nu_{1,3}$, ν_3, $\nu_{1,3} + \nu_{L'}$ and 2 $\nu_{1,3}$ of amorphous ice extracted from multiple scattering analysis of electron energy loss spectra. The white dots and triangle are measured integral cross sections for electron scattering from water in the gas phase: **a** elastic CSs ···○··· Danjo and Nishimura (1985); ···▽··· Johnstone and Newell (1991) and **b** cross sections for the ν_2, $\nu_{1,3}$ modes; ···○··· Seng and Linder (1976); ···▽··· Shyn et al. (1988) (Reproduced with permission from Michaud et al. (2003), © 2018 Radiation Research Society.)

structure similar to that of the elastic CSs. The CSs for quasielastic scattering of electron in amorphous ice, represented as the sum of the CSs for elastic scattering and that for excitation of translational phonon modes ($\nu_{T'}$ and $\nu_{T''}$) is shown in Fig. 1.5.

From their analysis Michaud et al., also obtained the vibrational CSs shown in Fig. 1.4b) for the 1–100 eV energy range (Michaud et al. 2003). As seen, the vibrational mode $\nu_{1,3}$, ν_2, ν_3, $\nu_{1,3} + \nu_{L'}$ and $2\nu_{1,3}$ exhibits a strong enhancement around 8 eV. This maximum is due to decay of the transient $^2B_2$ anion state into these modes. The energy position of this resonance is higher than the same resonance in the gas phase (i.e., 6–8 eV), which is thought to be due to the presence of hydrogen bonding in condensed phase (Michaud et al. 2003).

The sum of the CSs for other inelastic processes associated with greater energy losses than vibrational excitation (i.e., dissociative attachment (DA), electronic and ionization) is shown in Fig. 1.6 in the 1–100 eV energy range. There is a small maximum around 5.2 eV, in the energy dependence of these CSs, ascribed to the formation

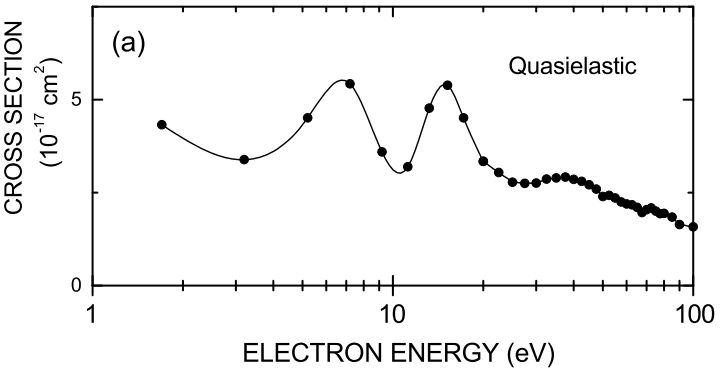

Fig. 1.5 Energy dependence of the integral cross sections of water given by the sum of the elastic and translational phonon $\nu_{T'}$ and $\nu_{T''}$ modes (Adapted from Michaud et al. (2003), © 2018 Radiation Research Society.)

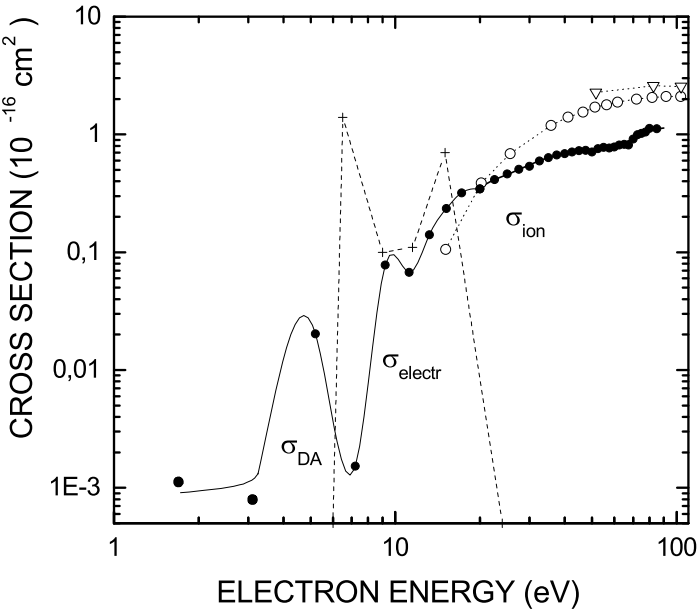

Fig. 1.6 Integral cross sections for dissociative electron attachment (DA), electronic excitation (electr) and ionization (ion) of amorphous ice (Reproduced from Michaud et al. (2003), © 2018 Radiation Research Society.)

of the $^2B_1$ transient negative ion state. Following this feature, there is a steady rise above 7.5 eV attributed to the electronic excitation and ionization processes.

Although the two-stream analysis of Michaud et al. considers electron scattering from individual isolated targets, the CSs derived from their work necessarily contains interference effects that modify the CS values. Since in amorphous ice, constructive or destructive interference is short range, the extracted values can be regarded as ensemble-averaged cross sections per scattering site, in the sense defined by Lekner and Cohen (Lekner 1967; Cohen and Lekner 1967) and Davis et al. (1971). Here, the scattering sites can be seen as those in the two-stream multiple scattering analysis. The extracted CSs include interference and screening effects originating from the surrounding molecules (Michaud and Sanche 1987a), which should be most pronounced in the elastic and quasi-elastic scattering CSs. In a first approximation, the ensemble-averaged integral quasieleastic scattering CS per scatterer can be expressed as

$$\sigma_{qe}(E_0) = \frac{m^2}{4\pi^2 h^4} \int_0^{2\pi} \int_0^{\pi} |V(K)|^2 S(K) \sin\theta d\theta d\varphi \tag{1.3}$$

where m is the reduced mass of the particle, $S(K)$ is the static structure factor of amorphous ice and $V(K)$ is the electron-molecule attraction potential. In the case of amorphous ice, the expression clearly shows that the gas-phase CSs are modulated by a structure factor taking into account short-range order diffraction. In fact, Michaud et al. have been able to correlate the results of Fig. 1.5 to the energy dependence of the structure factor (Michaud et al. 2003), showing that diffraction is occurring. Moreover, the structure factor decreases considerably with energy and, due to coherence, strongly reduces the quasi-elastic scattering CS below about 3 eV. In addition, Michaud et al. pointed out that a forward elastic scattering term is not contributing to the electron-beam attenuation in the two-stream analysis, which would make the derived elastic CSs, and thus the measured total CSs, smaller than they should be in amorphous ice. From this argument, Nikjoo et al. (2016) suggested to increase the published elastic CSs by factors derived from transport mean free paths, to produce values closer to those of the gas phase. Such factors are probably not needed for two reasons: (1) Eq. (1.3) can account for large reductions in the quasi-elastic CSs at low energies and (2) the higher momentum terms in the expansion of the scattered electron wavefunction are absent in the condensed phase due to the presence of neighboring molecules. This condition necessarily reduces the elastic and quasi-elastic scattering probabilities at each scattering site. Finally, we note that in similar investigations with disordered solid Xe films, the structure factor has been observed experimentally to reduce the gas-phase CS values by about an order of magnitude between 3 and 9 eV (Bader et al. 1982).

If CS values of amorphous ice are to be used for modelling liquid water, then they probably have to be increased to account for the reduction of coherence due

to enhancement of thermal phonon and vibrational excitation in the liquid phase, the different geometrical arrangement of the molecules and hydrogen bonding. A reasonable amplification factor of 2 was introduced empirically by Meesungnoen et al. (2002), when they applied the CSs of amorphous ice to their simulation of LEE elastic scattering in a water solution.

1.2.3.2 DNA Backbone: Deoxyribose and Phosphate Group

Figure 1.1 shows the structure of a DNA strand. The DNA backbone is comprised of two molecules: deoxyribose generally called the sugar group and the phosphate group. The most studied molecular analog of deoxyribose is tetrahydrofuran (THF—C_4H_8O) (Lepage et al. 1998; Antic et al. 1999, 2000; Breton et al. 2004; Bouchiha et al. 2006; Sulzer et al. 2006; Jäggle et al. 2006; Park et al. 2006). THF is a convenient model, since it represents the furyl ring at the center of the deoxyribose molecule, as seen in Fig. 1.7a). Lemelin et al. (2016b) measured absolute vibrational CSs for 1–19 eV electron scattering from THF using HREELS and the simple collision model described in Sect. 1.2.2.2. The vibrational CSs values were found to lie within the 10^{-17} cm^2 range. Figure 1.8 shows the energy dependence of the CSs. Highlighted in color are four features observed by the authors around 2.5, 4.5, 9.5 and 12.5 eV, which were all attributed to resonances. The maximum around 2.5 eV had not previously been predicted in theoretical calculations, but has been inferred in gas-phase studies (Allan 2007). Thus, its observation in this solid-phase study confirmed its existence and was attributed to the formation of a shape resonance. Considering the broadness of the other structures, the authors attributed these to shape or core-excited shape resonances. Pure core-excited resonances produce sharp features in scattering CSs; thus, they are rarely seen in vibrational CSs (Sanche and Schulz 1972). The three resonances at higher energy were also predicted or observed in other previous theoretical or experimental studies on LEEs interactions with THF (Lepage et al. 1998; Antic et al. 1999; Breton et al. 2004; Zecca et al. 2005; Trevisan et al. 2006; Winstead and McKoy 2006; Tonzani and Greene 2006; Allan 2007).

Absolute CSs were also measured for electronic excitations of THF by HREELS (Lemelin et al. 2016a). Spectra for energy losses between 6 and 11.5 eV were recorded

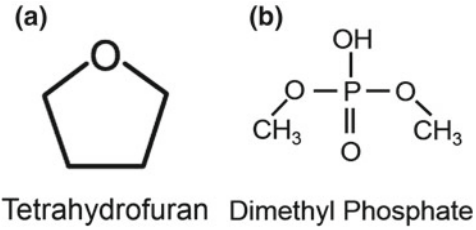

Fig. 1.7 Chemical structure of model molecules representing the sugar **a** Tetrahydrofuran (THF) and the phosphate group **b** Dimethyl Phosphate (DMP) of DNA

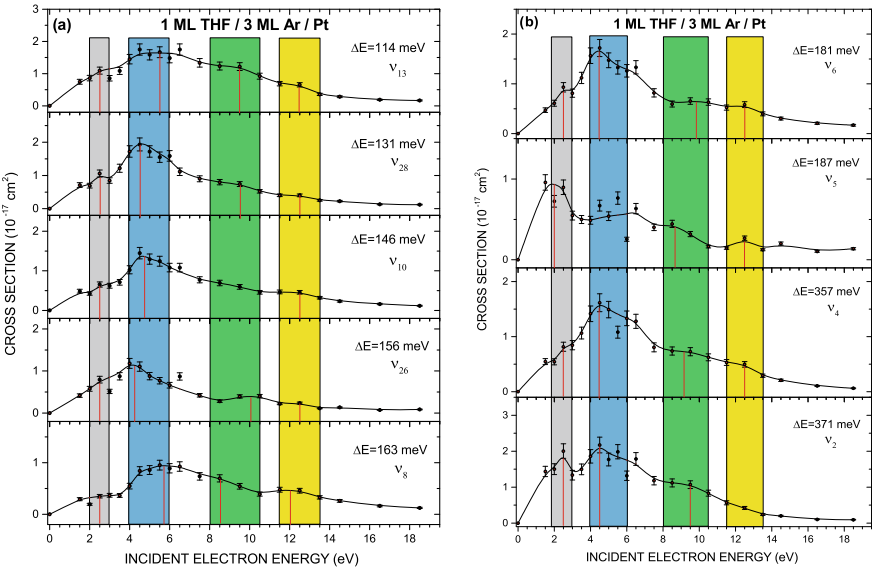

Fig. 1.8 Energy dependence of the absolute cross sections for various vibrational modes of tetrahydrofuran (THF) (Reproduced from Lemelin et al. (2016b), with the permission of AIP Publishing.)

for incident energies between 11 and 16 eV and a representative spectrum is shown in Fig. 1.9. Since unlike vibrational spectra, there were no readily identifiable energy loss peaks in the electronic spectra, fitting these latter with Gaussians functions to represent discrete electronic states, was unjustified. Instead, each spectrum was divided in five regions of 1 eV width and one remaining region of width 0.5 eV. Then, absolute CS values for each energy loss interval could be obtained from the area of the corresponding region using Eq. (1.1). The values of the CSs for each region lie within the 10^{-17} cm^2 range and are plotted as functions of E_0 in Fig. 1.10. No electron-resonance effects can be discerned in this figure. Furthermore, the CS values are lower than those measured for DNA bases or bases derivatives (see next subsection). These results are consistent with previous theoretical and experimental studies, which suggest that initial capture of an electron by DNA occurs on a base rather than on the backbone; subsequently, electron transfer to the backbone, can break a DNA strand (Barrios et al. 2002; Martin et al. 2004; Aflatooni et al. 2006; Sanche 2010; Caron and Sanche 2011).

A useful model of the phosphate group of DNA is dimethyl phosphate (DMP) shown in Fig. 1.7b). DMP consists of a phosphate group linked to two CH_3 which is rather like the DNA phosphate group that is linked to a CH and a CH_2. Absolute vibrational CSs have been measured for condensed DMP (Lemelin et al. 2017) using HREELS with the same technique and method described earlier (single collision treatment). They were acquired for electrons with incident energy of 1–18 eV. An example of EEL spectra of DMP is shown in Fig. 1.3. Each vibrational structure was identified and each spectrum was fitted to extract CSs. The energy dependence

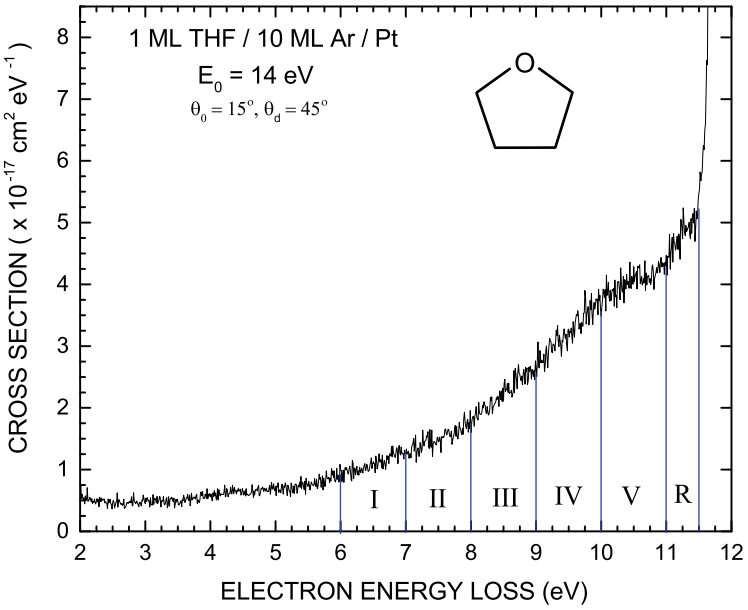

Fig. 1.9 EEL spectrum for electronic excitations of tetrahydrofuran recorded with incident electrons of 14 eV. No structure was clearly observed and fitting this spectrum with Gaussian distributions was not attempted. The spectrum is divided into 6 regions within which cross section values were extracted (Reproduced from Lemelin et al. (2016a), with the permission of AIP Publishing.)

of absolute vibrational CSs are presented in Fig. 1.11. It is possible to discern two strong electron resonances at low energies near 2 and 4 eV and two others of weaker magnitudes at higher energies near 7 and 12 eV. These structures can be compared to other resonances predicted or observed in prior theoretical and experimental studies with various phosphate group models (Pan and Sanche 2006; König et al. 2006; Aflatooni et al. 2006; Tonzani and Greene 2006; Burrow et al. 2008; Winstead and McKoy 2008; Bryjko et al. 2010; Bhaskaran and Sarma 2015). These resonances are likely pure shape resonances due to the broadness of the structures in the CS data.

1.2.3.3 DNA and RNA Bases Analogs

The DNA bases (or analogs) thymine, cytosine, adenine and pyrimidine have been studied with HREELS. Their absolute inelastic CSs, generated from the HREELS spectra, with the method described in Sect. 1.2.2.2 using the single collision model (Eq. (1.1)) are presented in this section.

Figure 1.12 shows the energy dependence of absolute vibrational CSs of condensed thymine for electrons with incident energies between 1 and 12 eV (Levesque et al. 2003). As seen, there is a common 2 eV wide structure around 4 eV for all of the vibrational modes of thymine. The maximum CS values is about 1.6×10^{-16} cm^2

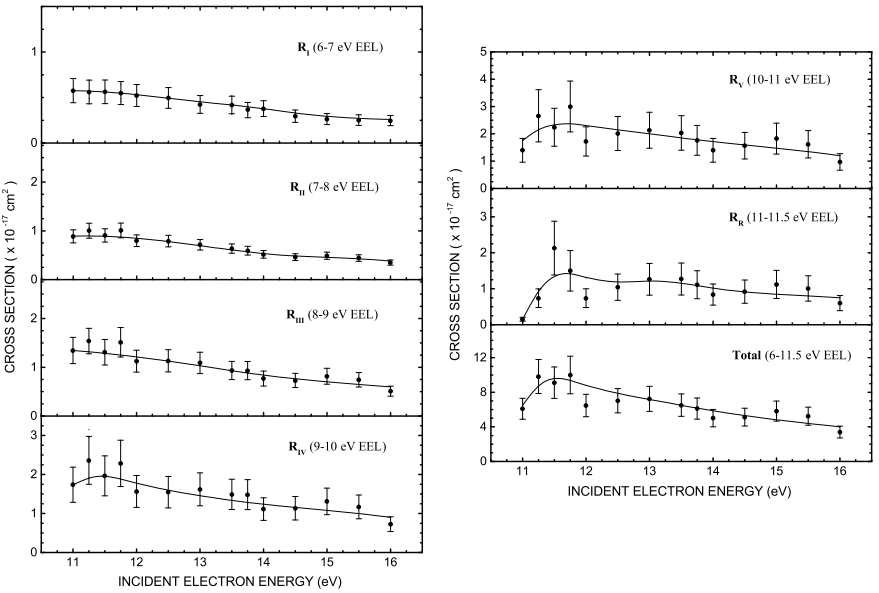

Fig. 1.10 Incident-electron-energy dependence of absolute cross sections for electronic excitations of THF in the 6 regions defined in the EEL spectrum of Fig. 1.9. The last graph represents the total cross section from the sum of energies loses from all regions (Reproduced from Lemelin et al. (2016a), with the permission of AIP Publishing.)

for the breathing mode (EEL of ~95 meV) at 4 eV and all the other CSs lie within the 10^{-17} cm^2 range. The feature at 4 eV is explained by the creation of a TNI by temporary trapping the incoming electron into the π^* orbital of thymine at 4.05 eV (Aflatooni et al. 1998) and its decay into vibrational excitations. The absolute CSs for electronic excitations of thymine have also been measured (Levesque et al. 2005a). The authors observed four electronic electron energy losses between 3.5 and 9 eV. The energy dependence of the absolute CSs associated with these modes are presented in Fig. 1.13. They observe two resonances: at low-energy around 5 eV with a CS of 2.9×10^{-17} cm^2 and at 8 eV with a maximum CS reaching 1.36×10^{-16} cm^2. These structures are related to the formation of TNIs and they correspond to the resonances at the same energies that have been reported in the O^- yield function from DEA to thymine in the gas phase (Huels et al. 1998). Thus, TNIs associated with the fragmentation of thymine can also decay into its electronic states.

In the case of cytosine (Michaud et al. 2012), absolute vibrational CSs have been reported for vibrational modes. The CS values are shown as a function of electron energy in Fig. 1.14, where four structures appear at 1.5, 3.5, 5.5 and 12 eV. These were also interpreted as arising from TNI formation by comparison with the features found in electron transmission spectra (Aflatooni et al. 1998) and DEA yield functions (Denifl et al. 2004; Aflatooni et al. 2006). The first two enhancements at 1.5 and 3.5 eV correspond to resonances found at 1.5 and 4.5 eV in gas-phase transmission

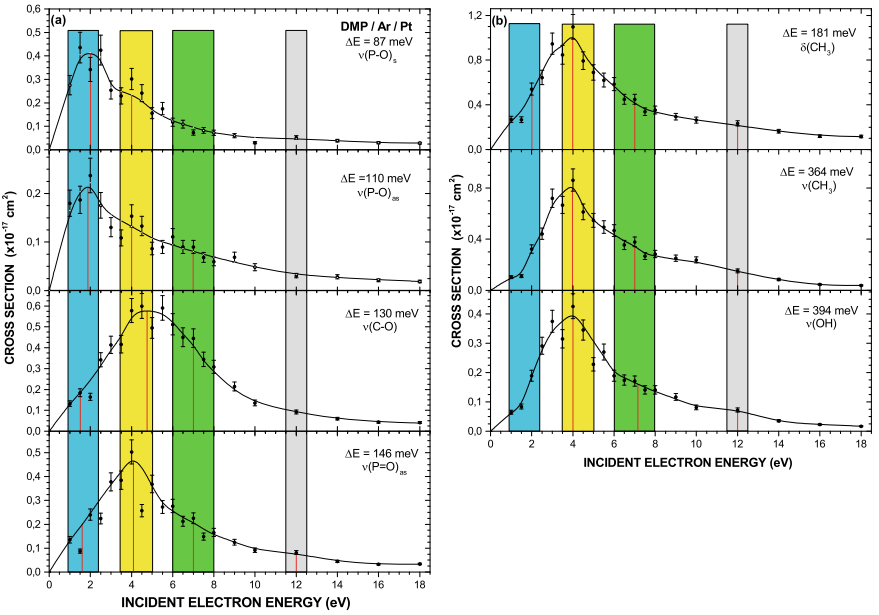

Fig. 1.11 Variation with electron collisional energy of the vibrational excitation cross sections of DMP (Reproduced from Lemelin et al. (2017), with the permission of AIP Publishing.)

Fig. 1.12 Absolute cross sections for different vibrational excitation modes of thymine as a function of electron incident energy (Reproduced with permission from Lévesque et al. (2003), with permission from Elsevier.)

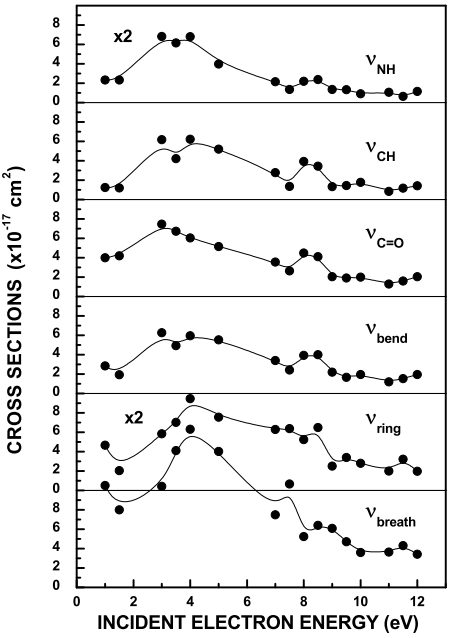

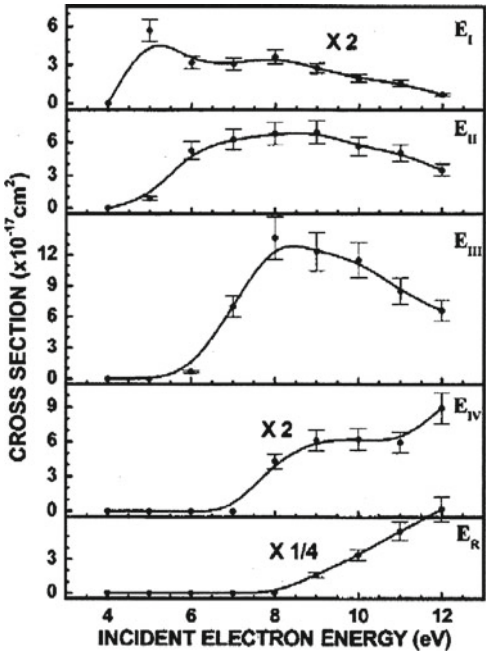

Fig. 1.13 Electron energy dependence of absolute cross sections for various electronic excitations (E_i) of thymine induce by 4–12 eV electron scattering (Reproduced from Lévesque et al. (2005a), with the permission of AIP Publishing.)

data. These resonances were ascribed to shape resonances. DEA studies on gas-phase cytosine also revealed three related resonances in the ranges of 1.5–2.1 eV, 5.2–6.8 eV, and 9.5–10.9 eV. It was then concluded that the TNIs responsible for these enhancements process have certain probabilities to decay into vibrational modes of cytosine. In addition, the absolute CSs for electronic excitations of cytosine have been measured (Bazin et al. 2010) for electron with energies between 5 and 18 eV. The authors observed eight electronic modes in HREEL spectra, from which they extracted the absolute CSs. They are all shown in Fig. 1.15. In the energy dependence of the CSs, they observe two resonances: a common maximum around 6 eV for the two lower excited states and another one near 10 eV. These TNIs correspond to the core-excited electron resonances found at the same energies (5.2–6.8 eV and 9.5–10.9 eV) in the gas-phase DEA channel (Denifl et al. 2004). The authors also measured the absolute CSs for four of the highest occupied orbitals of cytosine lying around 8.55, 9.21, 9.83 and 11.53 eV. The sum of their CSs are presented in Fig. 1.15 in the bottom right panel. This sum reaches a maximum of 8.1×10^{-16} cm^2 for incident electrons of 13 eV. As it appears in this graph, the theoretical calculations for the total ionization CSs are smaller below 15 eV, than the experimental values for electronic excitation. This result illustrates the relative importance of TNIs and their decay into electronic excitation at low energy.

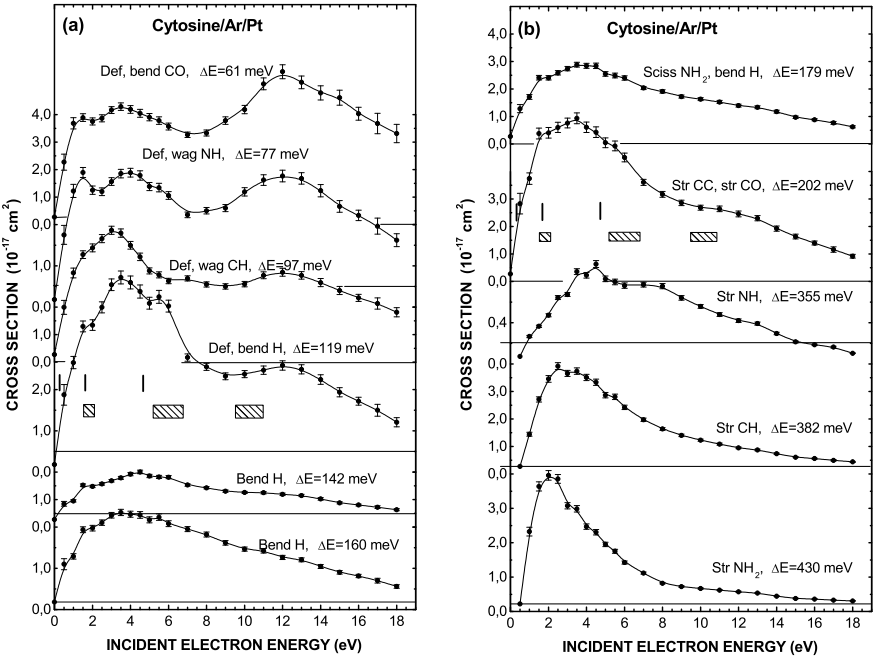

Fig. 1.14 Absolute cross sections for vibrational excitations of cytosine induced by 0.5–10 eV electron scattering (Reproduced from Michaud et al. (2012), with the permission of AIP Publishing.)

The base adenine is another important DNA constituent. Its vibrational excitation CSs measured (Panajotović et al. 2007) in the condensed phase by HREELS are shown in Fig. 1.16, where it is possible to observe a wide resonance for each vibrational mode in the range 3–5 eV. Also, a weak shoulder around 7 eV is present in the energy dependence of the vibrational absolute CSs for ring deformations and bending of hydrogen atoms. Shown in Fig. 1.17 is the energy dependence of the absolute CSs for electronic excitation by 8–12 eV electrons; a resonance can be seen around 10 eV in all decay channels.

The pyrimidine molecule has also been studied with HREELS in order to extract absolute vibrational and electronic excitation CSs (Levesque et al. 2005b). Pyrimidine is a relevant biomolecule or model to investigate its three nucleobases derivatives: cytosine, thymine and uracil. The energy dependence of the absolute vibrational CSs of pyrimidine is presented in Fig. 1.18 for five vibrational modes. As seen, the CSs exhibit a common 2 eV wide maximum in the 4–5 eV range. A shape resonance around 4 eV has been identified in electron transmission experiments of gas phase pyrimidine (Nenner and Schulz 1975) and compares well with energies of the structures in Fig. 1.18. In the ν_{9a}, ν_{18b} and ν_{CH} excitation modes, there is also a structure around 6 eV, which compares favorably with the energy of a resonance observed in the same transmission experiment (Nenner and Schulz 1975), as well as in the

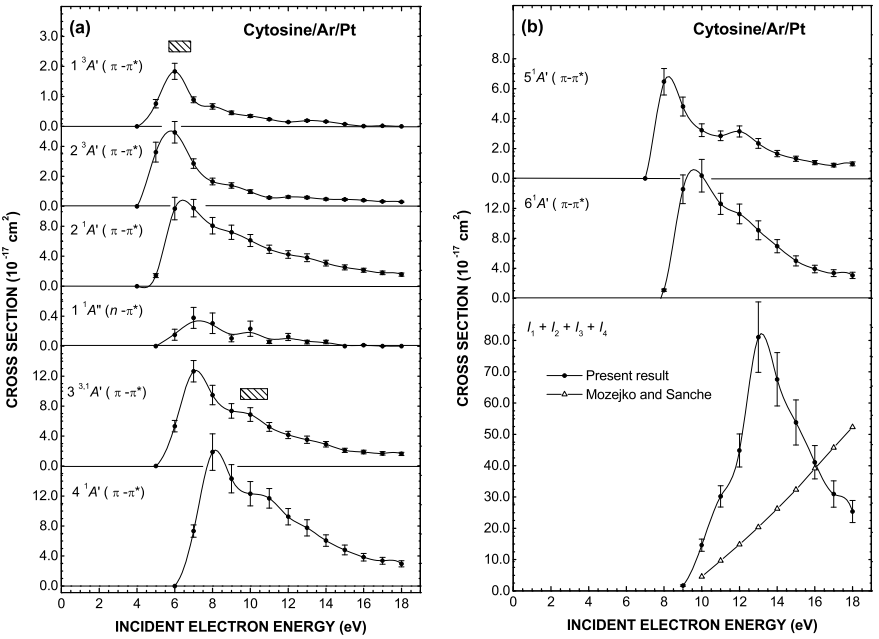

Fig. 1.15 Electron impact energy dependence of the cross sections to excite various electronic modes of cytosine within the range 4–15 eV (Reproduced from Bazin et al. (2010), with the permission of AIP Publishing.)

vibrational CSs of benzene (a closely related molecule to pyrimidine) found around 8 eV in the gas phase. This maximum has also been ascribed to the formation of a shape resonance (Burrow et al. 1987; Allan 1989; Arfa and Tronc 1990; Allan and Andric 1996). Finally, the numerical values of electronic excitation CSs of pyrimidine are presented in Table 1.1; there is no observable structure in energy dependence (Levesque et al. 2005b).

1.3 Nanodosimetry Using Absolute Cross Sections from HREELS Measurements

A simple application of LEE absolute CSs is presented in this section. This example demonstrates the relevance and potential for the determination of local doses by use of the absolute CSs values presented in the previous section. As mentioned in the introduction, new modalities such as TRT are currently being developed to target cancer cells with radiolabeled molecules and create local toxic and lethal doses to these cancer cells, while preserving healthy cells (Hayes 2017; Rezaee et al. 2017). TRT needs nanodosimetric modelling, which requires CSs (Itikawa and Mason 2005; Vinodkumar et al. 2006; Champion 2010; Anzai et al. 2012; Jones et al.

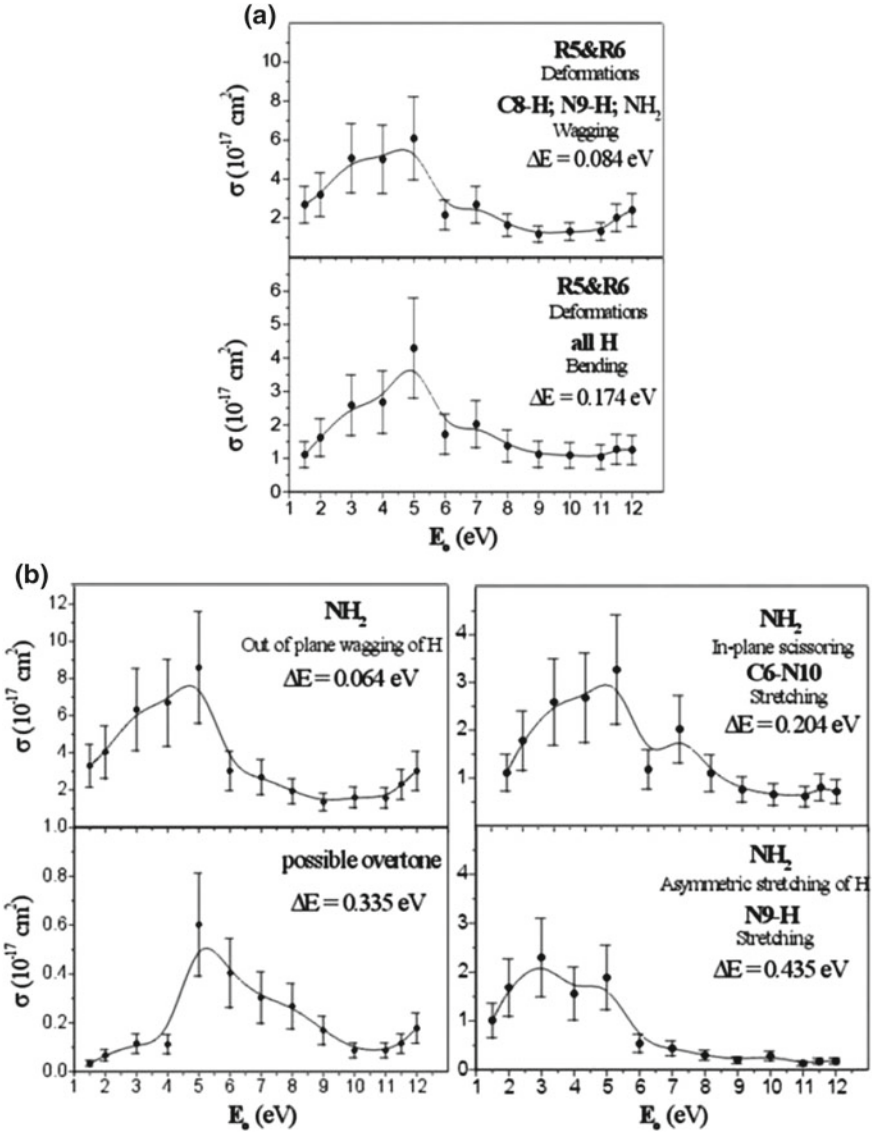

Fig. 1.16 Incident-electron-energy dependence of absolute cross sections for vibrational excitations of adenine within the range 1.5–12 eV. (Reproduced from Panajotović et al. (2007), with the permission of the Royal Society of Chemistry.)

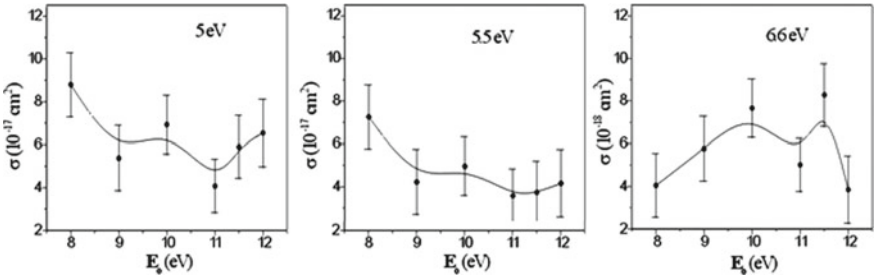

Fig. 1.17 Energy dependence of absolute cross sections for various electronic excitations of adenine induced by 8–12 eV electron scattering (Reproduced from Panajotović et al. (2007), with the permission of the Royal Society of Chemistry.)

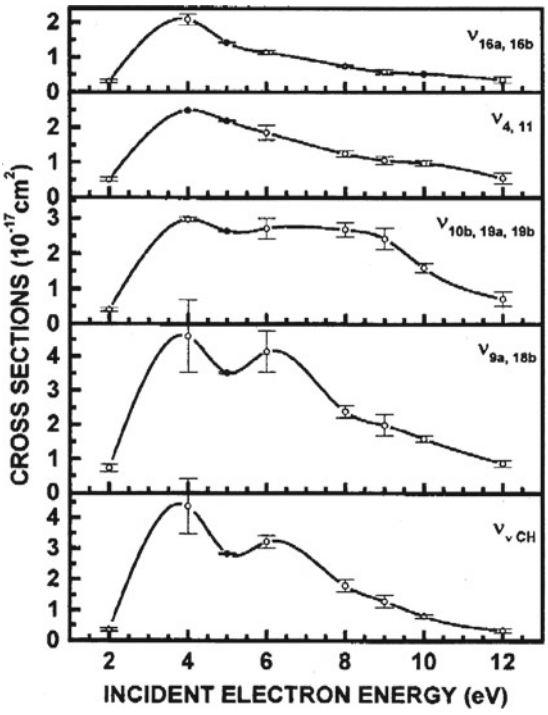

Fig. 1.18 Absolute vibrational excitation cross sections of pyrimidine induced by electron scattering in the range 2–12 eV (Reproduced from Lévesque et al. (2005b), with the permission of AIP Publishing.)

2012) to predict the energy deposited by LEEs and link that energy to radiobiological effectiveness (Nikjoo and Lindborg 2010).

An exclusive application of LEE absolute CSs was performed by Michaud et al. (2013). The goal was to present a simple method to assess the energy deposited near the site of a common targeting radioisotope (i.e., ^{125}I), using cytosine as a simple model for DNA. Figure 1.19 shows the geometry of a 1-nm-radius (R) cytosine shell with a ^{125}I nuclei lying at the center, which was used for calculations. The

Table 1.1 Cross sections (10^{-17} cm^2) at different incident energies E_0 (eV) for electrons exciting electronic states (E_i) of pyrimidine (Reproduced from Lévesque et al. (2005b), with the permission of AIP Publishing.)

	Electronic modes				
	E_I	E_{II}	E_{III}	E_{IV}	E_R
E_0	σ				
6	3.1	…	…	…	1.3
8	4.8	6.6	…	…	9.9
10	2.5	3.5	11.0	…	6.6
12	0.82	1.2	3.8	6.0	12.9

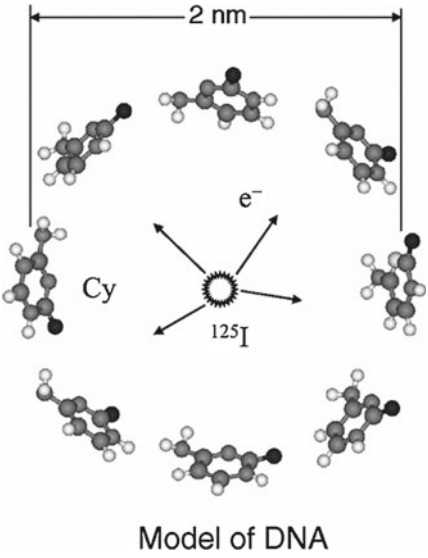

Fig. 1.19 Model for calculating nanoscopic doses imparted by LEEs, emitted from a radionuclide, to nearby biomolecules. In this example, a one-nm-radius spherical shell of cytosine is irradiated by a ^{125}I nuclei at its center (Reproduced with permission from Michaud et al. (2013), Copyright 2018 by the American Physical Society.)

absolute vibrational, electronic and ionization CSs of cytosine were entered into these calculations to estimate the energy deposited by LEEs into the cytosine shell following the decay of a ^{125}I nuclei.

The authors based their estimate of deposited dose on the energy spectrum of Auger electrons $N(E_0)$ released by the decay of ^{125}I as shown in Table 1.2. To generate the dose absorbed by the cytosine shell on such a nanoscopic scale, they employed the MIRD schema and the following equation (Loevinger et al. 1991):

$$S_{k\leftarrow h} = \frac{1}{4\pi R^2 m_{cy}} \sum_{E_{0,i}} N(E_0)\sigma_i(E_0)\epsilon_i. \tag{1.4}$$

Here $S_{k\leftarrow h}$ is the absorbed dose of target region k produced by a unit nuclear decay in the source region h (i.e., at the center of the cytosine shell) and ε_i is the energy of the

Table 1.2 Frequency distribution $N(E_0)$ as a function of the energy in eV (E_0) of the Auger electrons for a single nuclear decay of a single ^{125}I atom (Reproduced with permission from Michaud et al. (2013), Copyright 2018 by the American Physical Society.)

	$N(E_0)$																	
E_0	2	0.3	0.08	0.5	0	0.15	0.1	0.2	0.1	0.07	0.08	0.1	0.15	0	0.07	0.1	0.04	0.04
	1	2	3	4	5	6	7	8	9	10	11	12	13	14	15	16	17	18

excitation mode i of cytosine (i.e., vibrational, electronic excitation or ionization). $\sigma_i(E_0)$ is the integral CS to deposit energy ε_i into the excitations mode i and m_{cy} is the molecular mass of cytosine. The product $\sigma_i(E_0)\epsilon_i$ corresponds to the stopping CS (SCS) (Inokuti 1996). The SCSs can be calculated from the absolute CSs presented earlier in this chapter for cytosine; its energy dependence is presented in Fig. 1.20. The SCSs in this figure are divided in three categories for each type of excitations: vibrational, electronic and ionization. Using these SCSs as well as the frequency distribution of LEEs ($N(E_0)$) in Eq. (1.4), it is possible to calculate the dose absorbed by the cytosine shell for the decay of a ^{125}I at its center. The authors found that taking into account only the distribution of 0–18 eV electrons emanating from iodine, from a single decay of the isotope, 2.5, 31 and 45.5 kGy were absorbed by the shell due to vibrational and electronic excitations and ionization, respectively. Of course, the work of Michaud et al. only gives information on the energy deposited in the cytosine shell and does not correlate this quantity to possible damages made to the molecule in DNA, nor does it predicts the biological effects of this dose. Rather, this work provides an example of the nanodosimetry possible using absolute CSs and clearly demonstrates that, over a short range, LEEs can deposit an enormous dose.

The method was further elaborated by Rezaee et al. (2014), in a model of double-stranded DNA having the geometry shown in Fig. 1.19. These authors could correlate the absorbed dose deposited by LEEs to damage (Rezaee et al. 2014) in a 1 nm radius shell of double-stranded DNA with a ^{125}I nuclei at its center. They used all experimentally measured absolute CSs then available (supplemented with theoretical

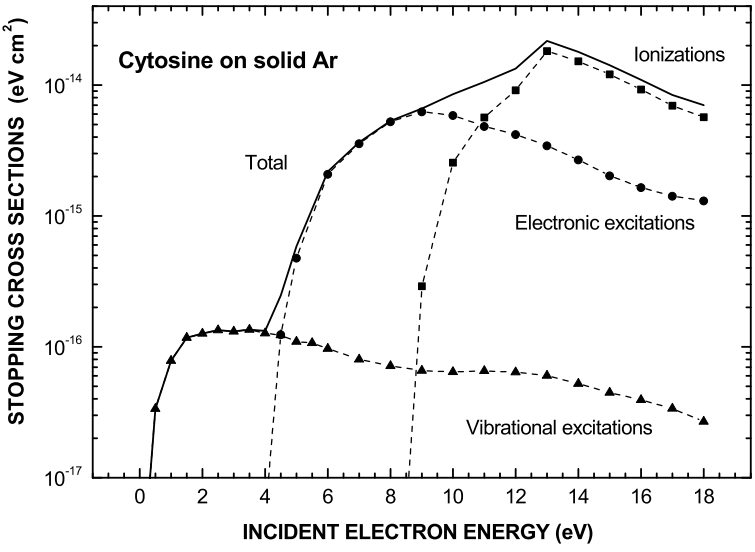

Fig. 1.20 Stopping cross sections for the vibrational and electronic excitations and ionizations of cytosine. These values were calculated from absolute cross sections of each process given in Figs. 1.14 and 1.15 (Reproduced with permission from Michaud et al. (2013), Copyright 2018 by the American Physical Society.)

data for unavailable CS) for DNA bases, THF and phosphate groups to model DNA strands of 8 nucleotides (4 base pairs). For a single decay of ^{125}I, the total dose absorbed by the 1 nm radius shell of hydrated and dry DNA was found to be about 272 and 205 kGy respectively, and resulted from the deposition of energy by LEEs via vibrational excitation, electronic excitation, and ionization. For hydrated DNA, the molecule was assumed to contain 20 water molecules per nucleotide. The energy range of LEEs considered was 5–18 eV.

In the same article, Rezaee et al. (2014) report damage CSs (DmCS) calculated from the energy dependence of the yields for the formation of SSBs and DSBs, which could be correlated to the efficiency of 5–18 eV Auger electrons (produced by the ^{125}I nuclei decay) to induce DNA strand breaks, in their 4-base DNA shell model. For a single nuclear decay of the radionuclide, the number of SSBs and DSBs induced by LEEs of energies between 5 and 18 eV was 0.5–0.02 respectively. This study amply demonstrated the short-range efficiency of LEEs in producing lethal cellular lesions. It also suggested that in nanometric volumes, the absorbed dose is no longer an appropriate physical parameter to represent biological effectiveness. In fact, the absorbed dose of LEEs in this study is 5 orders of magnitude larger than the dose absorbed in macro- and microscopic volumes, while the number of molecular lesions per unit dose is less than those in larger (macro- and microscopic) volumes (Goodhead 1994, 2006). However, the type of damage produced could have a greater impact at the biological level (e.g., cluster damages). In fact, since radiation interacts with matter in a stochastic way, a deterministic parameter like the absorbed dose has no meaning at the molecular level (Rezaee et al. 2014). For this reason, Rezaee et al. (2014) concluded that nanodosimetry and future radiotherapeutic modalities like TRT need to use both stopping and damage CSs, as biologically related physical parameters that can estimate the energy deposition and predict the damages at the nanometric level. Finally, these authors argued that their results illustrated how LEEs are as efficient as high-LET electrons and suggested that LEEs contribute considerably to the biological effects of radionuclides (Rezaee et al. 2014).

1.4 Future Trends

In Sect. 1.2.3, we presented absolute CSs for isolated fundamental units of DNA (i.e., each constituent was isolated from the others). When such species are combined into larger biomolecules, modifications of electron-molecule interactions are to be expected and thus also CSs values. Hence, the next logical step requires measurements of absolute CSs for LEEs scattering from larger biomolecules under more complex conditions. For example, it would be revealing to measure with HREELS the absolute CSs for a base linked to the deoxyribose (e.g., thymidine, cytidine, adenosine, etc.), and to compare the obtained CSs to those measured for each isolated constituent. It would give information on the effects of chemical bounding on the scattering process. Similarly, it would be interesting to investigate the effects of other molecules known to exist close to DNA in cells, for example water.

Rezaee et al. (2014) have previously discussed the effect of the presence of water molecules surrounding DNA. They refer to several studies (Rezaee et al. 2012; Boulanouar et al. 2013; Alizadeh and Sanche 2013), which have demonstrated that damage to DNA induced by LEEs is enhanced by the presence of water and oxygen. In recent years, a number of theoretical studies have incorporated additional water molecules into their calculations. For example, the review article of Kohanoff et al. (2017) discusses the effects microsolvation or solvation on electron-thymine interactions (Smyth and Kohanoff 2011; Smyth et al. 2014). It was shown (Smyth and Kohanoff 2011; Smyth et al. 2014) that as small a number as 5 water molecules linked to thymine by H-bonds, are sufficient to raise the energy required for dissociation of the molecule after the LEE attachment, relative to the gas phase. This phenomena has been observed experimentally with microhydrated uracil and thymine (Kočišek et al. 2016). One hypothesis to explain this result is that the DEA channel is supressed due to the redistribution of internal energy (caging) by the fast energy transfer to solvent, which leads to the stabilization of the intact anion (Kočišek et al. 2016). Hence, it becomes crucial to study the effect of water on CSs for various DNA constituents by HREELS or other methods. Data obtained with biomolecules surrounded by water molecules will surely be more relevant and more representative of the biological reality.

In cells, DNA is also surrounded by and linked to proteins. Thus, the close proximity of proteins to DNA also provides an interest in studying experimentally, the variation in inelastic LEE-scattering CSs caused by protein constituents close to DNA, such as certain amino acids. Moreover, any estimate of the DNA damage produced would necessarily have to include that caused by the radiation-induced radicals in the amino acids. Thus, LEE-damage CSs are also needed for amino acids. CSs for gas-phase amino acids have already been reported (Scheer et al. 2007); Glycine has been the most studied amino acid (Gohlke et al. 2002; Ptasinska et al. 2003; Lafosse et al. 2006; Esmaili et al. 2017, 2018). However, the configuration of amino acids in biological media can differ considerably from that in the gas phase. Indeed, these molecules adopt the zwitterion configuration in the presence of water (McNaught 1997; Lafosse et al. 2006). This configuration is highly polarized and hence expected to induce significant changes to the gas-phase LEE CSs. Obviously, electron CSs for amino acid in the condensed phase are needed, particularly in the presence of water.

Ultimately, one would like to measure absolute LEE-CSs for an entire DNA strand with HREELS. This is not an easy task, but Vilar et al. (2008) were able to measure and identify sharp vibrational excitation in the HREEL spectra of well-organized self-assembled monolayers (SAM) of single DNA strand. However, no data treatment was attempted to extract either differential or absolute CSs from these measurements. To extract absolute CSs from HREEL data using the single collision model, molecules must be randomly oriented on an inert surface (as explained in Sect. 1.2.2.2), preferably as a single or sub-monolayer film, which is definitely not the case of a DNA SAM. Hence, with this configuration, it is not possible to extract absolute CSs for DNA from HREEL spectra with our present formulation

of scattering within molecular and atomic solids. With present HREEL systems, it is not possible to sublimate DNA (under UHV) without breaking or damaging the molecule. In order to ultimately obtain condensed phase LEE-CSs for a DNA strand, more sophisticated methods of volatilisation must be implemented to create randomly oriented films of undamaged and condensed DNA strands. Laser-Induced Acoustic Desorption (LIAD) may be suitable for constructing such films, since it can sublimate large neutral biomolecules into the gas phase without damage (Golovlev et al. 1997; Shea et al. 2007). This method consists of depositing a solution of sample molecules (e.g., oligonucleotides) on a thin titanium foil and introducing this latter into an UHV chamber, where its reverse side is irradiated with a pulsed ND:YAG laser (Bald et al. 2008). The acoustic waves generated by the short laser pulse, travel to the coated side of the titanium foil, leading to the soft desorption of neutral and intact complex biomolecules (Golovlev et al. 1997; Shea et al. 2007). Bald et al. (2008) used LIAD method to vaporize thymidine in order to measure anion yields from DEA to this molecule in the gas-phase. They showed that no fragmentation was induced by LIAD. Thus, LIAD may have the potential to vaporize oligonucleotides, which could then be condensed onto a substrate. If LIAD is incorporated into a HREELS system, it could provide a powerful instrument to measure absolute CSs for LEE scattering from DNA.

1.5 Conclusion

HREELS is a powerful tool for studying the interactions of LEEs with biomolecules. This type of spectroscopy permits the extraction of absolute CSs for LEE energy losses to phononic, vibrational and electronic excitations. These CSs are required in nanodosimetric models related to the interaction of LEEs with biological media, as presented in this chapter. Dosimetric modelling is particularly needed for clinical modalities, where radionuclides are injected directly into a tumour or intravenously with a carrier molecule capable of targeting cancer cells or/and their nucleus. In these cases, to deliver a toxic and lethal dose directly and almost exclusively to cancer cells, the energy imparted at the nanoscopic level by the secondary species (e.g., LEEs) must be estimated. In this chapter, we have presented absolute CSs for the scattering of LEEs from DNA fundamental units and water molecules in the condensed phase.

Apart from the measurements of absolute LEE CSs for DNA subunits by HREELS, CSs for lethal cellular damages such as cross links, SSBs, DSBs and other cluster lesions can be measured experimentally using other techniques. These include X-rays photoelectrons spectroscopy (Klyachko et al. 1999; Briggs and Seah 2003), electron stimulated desorption (Abdoul-carime et al. 2000; Dugal et al. 2000), atomic force microscopy (AFM) (Bald and Keller 2014; Keller et al. 2015; Rackwitz et al. 2016, 2017; Schürmann et al. 2017) and electrophoresis (Rezaee et al. 2012). The increased availability of such CSs implemented in MC simulations should help reaching a fundamental understanding of the consequences of the passage of radia-

tion into cells and knowing more precisely the energy deposited and damage induced at the molecular level in cells.

While the CSs presented here are of crucial importance for radiotherapy, they may also have a positive impact in other related fields. Indeed, these absolute CSs could be used in radioprotection to estimate the risk of any radiation source on human health. This includes estimating the energy deposited in modalities using ionizing radiation for imaging body structures, tissues and biochemical processes (e.g. X-ray radiography or positron emission tomography (Brix et al. 2005; Einstein et al. 2007; Eisenberg et al. 2011; Fazel et al. 2016)). CSs for LEE interactions with biomolecules are also of relevance to space radiobiology. Cosmic radiations are among the greatest obstacles to manned interplanetary missions and the assessment and prediction of doses absorbed by astronauts are based on dosimetric models, including track-structure Monte Carlo simulations (Nikjoo et al. 2006, 2016; Dingfelder 2006; Plante and Cucinotta 2009; Durante and Cucinotta 2011; Kennedy 2014; Durante 2014). Exposure to high-energy galactic cosmic rays in space corresponds to a low dose rate (Zeitlin et al. 2013; Hassler et al. 2014), making it difficult to determine the biological effects from this parameter alone (Cucinotta et al. 2011; Chancellor et al. 2014; Norbury et al. 2016; Slaba et al. 2016). LEE CSs values should aid in this fundamental comprehension, arising from models, to correlate the energy deposition at the nanoscopic level within cells to the biological effects of low-dose exposures.

References

Abdoul-carime AH, Dugal P, Sanche L (2000) Damage induced by 1–30 eV electrons on thymine- and bromouracil-substituted oligonucleotides linked references are available on JSTOR for this article: damage Induced by 1–30 eV electrons on thymine- and bromouracil-substituted oligonucleotides. Radiat Res Soc 153:23–28

Aflatooni K, Gallup GA, Burrow PD (1998) Electron attachment energies of the DNA bases. J Phys Chem A 102:6205–6207. https://doi.org/10.1021/jp980865n

Aflatooni K, Scheer AM, Burrow PD (2006) Total dissociative electron attachment cross sections for molecular constituents of DNA. J Chem Phys 125:54301. https://doi.org/10.1063/1.2229209

Alizadeh E, Sanche L (2013) Role of humidity and oxygen level on damage to DNA induced by soft X-rays and low-energy electrons. J Phys Chem C 117:22445–22453. https://doi.org/10.1021/jp403350j

Allan M (1989) Study of triplet states and short-lived negative ions by means of electron impact spectroscopy. J Electron Spectros Relat Phenomena 48:219–351. https://doi.org/10.1016/0368-2048(89)80018-0

Allan M (2007) Absolute angle-differential elastic and vibrational excitation cross sections for electron collisions with tetrahydrofuran. J Phys B: At Mol Opt Phys 40:3531–3544. https://doi.org/10.1088/0953-4075/40/17/020

Allan M, Andric L (1996) Σ* resonances in electron impact-induced vibrational excitation of N-propane, cyclopropane, ethylene oxide, cyclopentane, and cyclohexane. J Chem Phys 105:3559–3568. https://doi.org/10.1063/1.472819

Alloni D, Campa A, Friedland W et al (2012) Track structure, radiation quality and initial radiobiological events: considerations based on the PARTRAC code experience. Int J Radiat Biol 88:77–86. https://doi.org/10.3109/09553002.2011.627976

Antic D, Parenteau L, Lepage M, Sanche L (1999) Low-energy electron damage to condensed-phase deoxyribose analogues investigated by electron stimulated desorption of H—and electron energy loss spectroscopy. J Phys Chem B 103:6611–6619. https://doi.org/10.1021/jp990686l

Antic D, Parenteau L, Sanche L (2000) Electron-stimulated desorption of H—from condensed-phase deoxyribose analogues: dissociative electron attachment versus resonance decay into dipolar dissociation. J Phys Chem B 104:4711–4716. https://doi.org/10.1021/jp000206m

Anzai K, Kato H, Hoshino M et al (2012) Cross section data sets for electron collisions with H_2, O_2, CO, CO_2, N_2O and H_2O. Eur Phys J D 66:36. https://doi.org/10.1140/epjd/e2011-20630-1

Arfa MB, Tronc M (1990) Symmetry selection rules vs. vibronic coupling in resonant selective vibrational excitation of polyatomic molecules by electron impact. J Electron Spectros Relat Phenomena 50:117–128. https://doi.org/10.1016/0368-2048(90)80013-Z

Arumainayagam CR, Lee HL, Nelson RB et al (2010) Low-energy electron-induced reactions in condensed matter. Surf Sci Rep 65:1–44. https://doi.org/10.1016/j.surfrep.2009.09.001

Bader G, Perluzzo G, Caron LG, Sanche L (1982) Elastic and inelastic mean-free-path determination in solid xenon from electron transmission experiments. Phys Rev B 26:6019–6029. https://doi.org/10.1103/physrevb.26.6019

Bader G, Chiasson J, Caron LG et al (1988) Absolute scattering probabilities for subexcitation electrons in condensed H_2O. Radiat Res 114:467–479. https://doi.org/10.2307/3577118

Bald I, Keller A (2014) Molecular processes studied at a single-molecule level using DNA origami nanostructures and atomic force microscopy. Molecules 19:13803–13823. https://doi.org/10.3390/molecules190913803

Bald I, Dąbkowska I, Illenberger E (2008) Probing biomolecules by laser-induced acoustic desorption: electrons at near zero electron volts trigger sugar-phosphate cleavage. Angew Chemie Int Ed 47:8518–8520. https://doi.org/10.1002/anie.200803382

Barrios R, Skurski P, Simons J (2002) Mechanism for damage to DNA by low-energy electrons †. J Phys Chem B 106:7991–7994. https://doi.org/10.1021/jp013861i

Bass AD, Sanche L (1998) Absolute and effective cross-sections for low-energy electron-scattering processes within condensed matter. Radiat Environ Biophys 37:243–257. https://doi.org/10.1007/s004110050125

Bauer E (1994) Low energy electron microscopy. Reports Prog Phys 57:895–938

Bazin M, Michaud M, Sanche L (2010) Absolute cross sections for electronic excitations of cytosine by low energy electron impact. J Chem Phys 133:155104. https://doi.org/10.1063/1.3505301

Bennett CJ, Kaiser RI (2007) On the formation of glycolaldehyde ($HCOCH_2OH$) and methyl formate ($HCOOCH_3$) in interstellar ice analogs. Astrophys J 661:899–909. https://doi.org/10.1086/516745

Bhaskaran R, Sarma M (2015) Low-energy electron interaction with the phosphate group in DNA molecule and the characteristics of single-strand break pathways. J Phys Chem A 119:10130–10136. https://doi.org/10.1021/acs.jpca.5b08000

Bouchiha D, Gorfinkiel JD, Caron LG, Sanche L (2006) Low-energy electron collisions with tetrahydrofuran. J Phys B: At Mol Opt Phys 39:975–986. https://doi.org/10.1088/0953-4075/39/4/021

Boudaïffa B, Cloutier P, Hunting D et al (2000) Resonant formation of DNA strand breaks by low-energy (3 to 20 eV) electrons. Science (80-) 287:1658–1660

Boulanouar O, Fromm M, Bass AD et al (2013) Absolute cross section for loss of supercoiled topology induced by 10 eV electrons in highly uniform/DNA/1,3-diaminopropane films deposited on highly ordered pyrolitic graphite. J Chem Phys 139:55104. https://doi.org/10.1063/1.4817323

Breton S-P, Michaud M, Jäggle C et al (2004) Damage induced by low-energy electrons in solid films of tetrahydrofuran. J Chem Phys 121:11240. https://doi.org/10.1063/1.1814632

Briggs D, Seah MP (2003) Practical surface analysis: by auger and X-ray photoelectron spectroscopy. Wiley

Brix G, Lechel U, Glatting G et al (2005) Radiation exposure of patients undergoing whole-body dual-modality 18F-FDG PET/CT examinations. J Nucl Med 46:608–614

Bryjko L, van Mourik T, Dora A, Tennyson J (2010) R-matrix calculation of low-energy electron collisions with phosphoric acid. J Phys B: At Mol Opt Phys 43:235203. https://doi.org/10.1088/0953-4075/43/23/235203

Burrow PD, Michejda JA, Jordan KD (1987) Electron transmission study of the temporary negative ion states of selected benzenoid and conjugated aromatic hydrocarbons. J Chem Phys 86:9–24. https://doi.org/10.1063/1.452598

Burrow PD, Gallup GA, Modelli A (2008) Are there π* shape resonances in electron scattering from phosphate groups? J Phys Chem A 112:4106–4113. https://doi.org/10.1021/jp7109143

Caron LG, Sanche L (2011) Theoretical studies of electron interactions with DNA and its subunits: from tetrahydrofuran to plasmid DNA. In: Carsky P, Curik R (eds) Low-energy electron scattering from molecules. CRC Press, Biomolecules and Surfaces, pp 161–230

Champion C (2010) Electron impact ionization of liquid and gaseous water: a single-center partial-wave approach. Phys Med Biol 55:11–32. https://doi.org/10.1088/0031-9155/55/1/002

Chancellor J, Scott G, Sutton J (2014) Space radiation: the number one risk to astronaut health beyond low earth orbit. Life 4:491–510. https://doi.org/10.3390/life4030491

Chattopadhyay N, Cai Z, Pignol J-P et al (2010) Design and characterization of HER-2-targeted gold nanoparticles for enhanced X-radiation treatment of locally advanced breast cancer. Mol Pharm 7:2194–2206. https://doi.org/10.1021/mp100207t

Chattopadhyay N, Cai Z, Kwon YL et al (2013) Molecularly targeted gold nanoparticles enhance the radiation response of breast cancer cells and tumor xenografts to X-radiation. Breast Cancer Res Treat 137:81–91. https://doi.org/10.1007/s10549-012-2338-4

Chen W, Chen S, Dong Y et al (2016) Absolute cross-sections for DNA strand breaks and crosslinks induced by low energy electrons. Phys Chem Chem Phys 18:32762–32771. https://doi.org/10.1039/c6cp05201k

Chiari L, Duque HV, Jones DB et al (2014) Differential cross sections for intermediate-energy electron scattering from α-tetrahydrofurfuryl alcohol: excitation of electronic-states. J Chem Phys 141:24301. https://doi.org/10.1063/1.4885856

Cohen MH, Lekner J (1967) Theory of hot electrons in gases, liquids, and solids. Phys Rev 158:305–309. https://doi.org/10.1103/physrev.158.305

Connell PP, Hellman S (2009) Advances in radiotherapy and implications for the next century: a historical perspective. Cancer Res 69:383–392. https://doi.org/10.1158/0008-5472.can-07-6871

Conrad H, Kordesch ME (2017) High resolution electron energy loss spectroscopy, applications. In: Lindon JC, Tranter GE, Koppenaal DW (eds) Encyclopedia of spectroscopy and spectrometry, 2nd edn. Elsevier, Oxford, pp 47–57

Cucinotta F, Kim M, Chappell L (2011) Space radiation cancer risk projections and uncertainties-2010. NASA Tech Pap 1–132

Danjo A, Nishimura H (1985) Elastic scattering of electrons from H_2O molecule. J Phys Soc Japan 54:1224–1227. https://doi.org/10.1143/jpsj.54.1224

Davis HT, Schmidt LD, Minday RM (1971) Kinetic theory of excess electrons in polyatomic gases, liquids, and solids. Phys Rev A 3:1027–1037. https://doi.org/10.1103/physreva.3.1027

Denifl S, Ptasińska S, Probst M et al (2004) Electron attachment to the gas-phase DNA bases cytosine and thymine. J Phys Chem A 108:6562–6569. https://doi.org/10.1021/jp049394x

Dingfelder M (2006) Track structure: time evolution from physics to chemistry. Radiat Prot Dosimetry 122:16–21. https://doi.org/10.1093/rpd/ncl494

Dingfelder M, Travia A, Mclawhorn RA et al (2009) Electron emission from foils and biological materials after proton impact. Radiat Phys Chem Oxf Engl 1993 77:1213–1217. https://doi.org/10.1016/j.radphyschem.2008.05.046.electron

Douglass M, Penfold S, Bezak E (2015) Preliminary investigation of microdosimetric track structure physics models in Geant4-DNA and RITRACKS. Comput Math Methods Med 2015. https://doi.org/10.1155/2015/968429

Dugal P-C, Abdoul-Carime H, Sanche L (2000) Mechanisms for low-energy (0.5–30 eV) electron-induced pyrimidine ring fragmentation within thymine- and halogen-substituted single strands of DNA. J Phys Chem B 104:5610–5617. https://doi.org/10.1021/jp9938112

Duque HV, Do TPT, Lopes MCA et al (2015) The role of electron-impact vibrational excitation in electron transport through gaseous tetrahydrofuran. J Chem Phys 142:124307. https://doi.org/10.1063/1.4915889

Durante M (2014) Space radiation protection: destination Mars. Life Sci Sp Res 1:2–9. https://doi.org/10.1016/j.lssr.2014.01.002

Durante M, Cucinotta FA (2011) Physical basis of radiation protection in space travel. Rev Mod Phys 83:1245–1281. https://doi.org/10.1103/revmodphys.83.1245

Einstein AJ, Moser KW, Thompson RC et al (2007) Radiation dose to patients from cardiac diagnostic imaging. Circulation 116:1290–1305

Eisenberg MJ, Afilalo J, Lawler PR et al (2011) Cancer risk related to low-dose ionizing radiation from cardiac imaging in patients after acute myocardial infarction. CMAJ 183:430–436. https://doi.org/10.1503/cmaj.100463

Emfietzoglou D, Cucinotta FA, Nikjoo H (2005) A complete dielectric response model for liquid water: a solution of the Bethe ridge problem. Radiat Res 164:202–211. https://doi.org/10.1667/rr3399

Esmaili S, Bass AD, Cloutier P et al (2017) Synthesis of complex organic molecules in simulated methane rich astrophysical ices. J Chem Phys 147. https://doi.org/10.1063/1.5003898

Esmaili S, Bass AD, Cloutier P et al (2018) Glycine formation in CO_2 : CH_4 : NH_3 ices induced by 0–70 eV electrons. 164702:0–8. https://doi.org/10.1063/1.5021596

Fazel R, Krumholz HM, Wang Y et al (2016) Exposure to low-dose ionizing radiation from medical imaging procedures. Emerg Nurse 24:15. https://doi.org/10.1056/nejmp1002530

Francis Z, Incerti S, Karamitros M et al (2011) Stopping power and ranges of electrons, protons and alpha particles in liquid water using the Geant4-DNA package. Nucl Instrum Methods Phys Res Sect B Beam Interact with Mater Atoms 269:2307–2311. https://doi.org/10.1016/j.nimb.2011.02.031

Francis Z, Incerti S, Ivanchenko V et al (2012) Monte Carlo simulation of energy-deposit clustering for ions of the same LET in liquid water. Phys Med Biol 57:209–224. https://doi.org/10.1088/0031-9155/57/1/209

Gaze MN (1996) The current status of targeted radiotherapy in clinical practice. Phys Med Biol 41:1895

Ghandi K, Wang F, Landry C, Mehran Mostafavi (2018) Naked gold nanoparticles and hot electrons in water. Sci Rep 1–6. https://doi.org/10.1038/s41598-018-25711-2

Gohlke S, Rosa A, Illenberger E et al (2002) Formation of anion fragments from gas-phase glycine by low energy (0–15 eV) electron impact. J Chem Phys 116:10164–10169. https://doi.org/10.1063/1.1479348

Golovlev VV, Allman SL, Garrett WR, Chen CH (1997) Laser-induced acoustic desorption of electrons and ions. Appl Phys Lett 71:852–854. https://doi.org/10.1063/1.119667

Goodhead DT (1994) Initial events in the cellular effects of ionizing radiations: clustered damage in DNA. Int J Radiat Biol 65:7–17. https://doi.org/10.1080/09553009414550021

Goodhead DT (2006) Energy deposition stochastics and track structure: what about the target? Radiat Prot Dosimetry 122:3–15. https://doi.org/10.1093/rpd/ncl498

Hainfeld JF, Slatkin DN, Smilowitz HM (2004) The use of gold nanoparticles to enhance radiotherapy in mice. Phys Med Biol 49. https://doi.org/10.1088/0031-9155/49/18/n03

Hainfeld JF, Dilmanian FA, Slatkin DN, Smilowitz HM (2008) Radiotherapy enhancement with gold nanoparticles. J Pharm Pharmacol 60:977–985. https://doi.org/10.1211/jpp.60.8.0005

Hainfeld JF, Dilmanian FA, Zhong Z et al (2010) Gold nanoparticles enhance the radiation therapy of a murine squamous cell carcinoma. Phys Med Biol 55:3045–3059. https://doi.org/10.1088/0031-9155/55/11/004

Hall EJ, Wuu CS (2003) Radiation-induced second cancers: the impact of 3D-CRT and IMRT. Int J Radiat Oncol Biol Phys 56:83–88. https://doi.org/10.1016/s0360-3016(03)00073-7

Hassler DM, Zeitlin C, Wimmer-Schweingruber RF et al (2014) Mars' surface radiation environment measured with the Mars Science Laboratory's Curiosity Rover. Science (80-) 343:1244797–1244797. https://doi.org/10.1126/science.1244797

Hayes AC (2017) Applications of nuclear physics. Reports Prog Phys 80. https://doi.org/10.1088/1361-6633/80/2/026301

Hervé Du Penhoat MA, Huels MA, Cloutier P et al (2001) Electron stimulated desorption of H- from thin films of thymine and uracil. J Chem Phys 114:5755–5764. https://doi.org/10.1063/1.1349707

Holtom PD, Bennett CJ, Osamura Y et al (2005) A combined experimental and theoretical study on the formation of the amino acid glycine (NH_2CH_2COOH) and its isomer ($CH_3NHCOOH$) in extraterrestrial ices. Astrophys J 626:940–952. https://doi.org/10.1086/430106

Huels MA, Hahndorf I, Illenberger E, Sanche L (1998) Resonant dissociation of DNA bases by subionization electrons resonant dissociation of DNA bases by subionization electrons. 108:1309. https://doi.org/10.1063/1.475503

Huels MA, Boudaiffa B, Cloutier P et al (2003) Single, double, and multiple double strand breaks induced in DNA by 3–100 eV electrons. J Am Chem Soc 125:4467–4477

Hyun Cho S, Jones BL, Krishnan S (2005) Physics in medicine & biology estimation of tumour dose enhancement due to gold nanoparticles during typical radiation treatments: a preliminary Monte Carlo study. The dosimetric feasibility of GNRT. Sang Hyun Cho Phys Med Biol 50. https://doi.org/10.1088/0031-9155/50/15/n01

Ibach H, Mills DL (1982) Electron energy loss spectroscopy and surface vibrations. Academic, Elsevier Science, New York

Inokuti M (1983) Radiation physics as basis of radiation chemistry and biology. In: Applied atomic collision physics. Academic Press, New-York, pp 179–236

Inokuti M (1996) Remarks on stopping power: its connections with particle transport and with the electronic structure of matter. Int J Quantum Chem 57:173–182

Itikawa Y, Mason N (2005) Cross sections for electron collisions with water molecules. J Phys Chem Ref Data 34:1–22. https://doi.org/10.1063/1.1799251

Jäggle C, Swiderek P, Breton S-P et al (2006) Products and reaction sequences in tetrahydrofuran exposed to low-energy electrons. J Phys Chem B 110:12512–12522. https://doi.org/10.1021/jp0614291

Johnstone WM, Newell WR (1991) Absolute vibrationally elastic cross sections for electrons scattered from water molecules between 6 eV and 50 eV. J Phys B: At Mol Opt Phys 24:3633–3643. https://doi.org/10.1088/0953-4075/24/16/015

Jones DB, Bellm SM, Blanco F et al (2012) Differential cross sections for the electron impact excitation of pyrimidine. J Chem Phys 137:74304. https://doi.org/10.1063/1.4743961

Kaiser RI (2002) Experimental investigation on the formation of carbon-bearing molecules in the interstellar medium via neutral-neutral reactions. Chem Rev 102:1309–1358. https://doi.org/10.1021/cr970004v

Keller A, Rackwitz J, Cauët E et al (2015) Sequence dependence of electron-induced DNA strand breakage revealed by DNA nanoarrays. Sci Rep 4:7391. https://doi.org/10.1038/srep07391

Kennedy AR (2014) Biological effects of space radiation and development of effective countermeasures. Life Sci Space Res 1:10–43. https://doi.org/10.1016/j.lssr.2014.02.004

Klyachko DV, Huels MA, Sanche L, Sanche L (1999) Halogen anion formation in 5-halouracil films: X rays compared to subionization electrons. Radiat Res 151:177. https://doi.org/10.2307/3579768

Kočišek J, Pysanenko A, Fárník M, Fedor J (2016) Microhydration prevents fragmentation of uracil and thymine by low-energy electrons. J Phys Chem Lett 7:3401–3405. https://doi.org/10.1021/acs.jpclett.6b01601

Kohanoff J, McAllister M, Tribello GA, Gu B (2017) Interactions between low energy electrons and DNA: a perspective from first-principles simulations. J Phys: Condens Matter 29:383001. https://doi.org/10.1088/1361-648x/aa79e3

Kong T, Zeng J, Wang X et al (2008) Enhancement of radiation cytotoxicity in breast-cancer cells by localized attachment of gold nanoparticles. Small 4:1537–1543. https://doi.org/10.1002/smll.200700794

König C, Kopyra J, Bald I, Illenberger E (2006) Dissociative electron attachment to phosphoric acid esters: the direct mechanism for single strand breaks in DNA. Phys Rev Lett 97:18105. https://doi.org/10.1103/physrevlett.97.018105

Kyriakou I, Emfietzoglou D, Ivanchenko V et al (2017) Microdosimetry of electrons in liquid water using the low-energy models of Geant4. J Appl Phys 122. https://doi.org/10.1063/1.4992076

Lafosse A, Azria R (2011) Low-energy electron scattering at surfaces. In: Čurík R, Čársky P (eds) Low-energy electron scattering from molecules. CRC Press, Biomolecules and Surfaces, pp 231–262

Lafosse A, Bertin M, Domaracka A et al (2006) Reactivity induced at 25 K by low-energy electron irradiation of condensed NH 3 –CH 3 COOD (1: 1) mixture. Phys Chem Chem Phys 8:5564–5568. https://doi.org/10.1039/b613479c

Lechtman E, Chattopadhyay N, Cai Z et al (2011) Implications on clinical scenario of gold nanoparticle radiosensitization in regards to photon energy. Phys Med Biol 56:4631–4647. https://doi.org/10.1088/0031-9155/56/15/001

Lekner J (1967) Motion of electrons in liquid argon. Phys Rev 158:130–137. https://doi.org/10.1103/physrev.158.130

Lemelin V, Bass AD, Cloutier P, Sanche L (2016a) Absolute cross sections for electronic excitation of condensed tetrahydrofuran (THF) by 11–16 eV electrons. J Chem Phys 145:174703. https://doi.org/10.1063/1.4966650

Lemelin V, Bass AD, Cloutier P, Sanche L (2016b) Absolute vibrational cross sections for 1–19 eV electron scattering from condensed tetrahydrofuran (THF). J Chem Phys 144:74701. https://doi.org/10.1063/1.4941377

Lemelin V, Bass AD, Wagner JR, Sanche L (2017) Absolute vibrational excitation cross sections for 1–18 eV electron scattering from condensed dimethyl phosphate (DMP). J Chem Phys 147:234305. https://doi.org/10.1063/1.5008486

Lepage M, Letarte S, Michaud M et al (1998) Electron spectroscopy of resonance-enhanced vibrational excitations of gaseous and solid tetrahydrofuran. J Chem Phys 109:5980–5986. https://doi.org/10.1063/1.477223

Lepage M, Michaud M, Sanche L (2000) Low-energy electron-energy-loss spectroscopy of condensed acetone: electronic transitions and resonance-enhanced vibrational excitations. J Chem Phys 112:6707–6715. https://doi.org/10.1063/1.481245

Levesque PL, Michaud M, Sanche L (2003) Cross sections for low energy (1–12 eV) inelastic electron scattering from condensed thymine. Nucl Instrum Methods Phys Res Sect B Beam Interact with Mater Atoms 208:225–230. https://doi.org/10.1016/s0168-583x(03)00661-x

Levesque PL, Michaud M, Cho W, Sanche L (2005a) Absolute electronic excitation cross sections for low-energy electron (5–12 eV) scattering from condensed thymine. J Chem Phys 122:224704. https://doi.org/10.1063/1.1925610

Levesque PL, Michaud M, Sanche L (2005b) Absolute vibrational and electronic cross sections for low-energy electron (2–12 eV) scattering from condensed pyrimidine. J Chem Phys 122:94701. https://doi.org/10.1063/1.1854121

Liljequist D, Liamsuwan T, Nikjoo H (2012) Elastic scattering cross section models used for Monte Carlo simulation of electron tracks in media of biological and medical interest. Int J Radiat Biol 88:29–37. https://doi.org/10.3109/09553002.2011.584943

Loevinger R, Budinger TF, Watson EE (1991) MIRD primer for absorbed dose calculations, revised edition. The Society of Nuclear Medicine, Inc., New York

Lozano AI, Krupa K, Ferreira da Silva F et al (2017) Low energy electron transport in furfural. Eur Phys J D 71:226. https://doi.org/10.1140/epjd/e2017-80326-0

Lu QB, Sanche L (2001) Effects of cosmic rays on atmospheric chlorofluorocarbon dissociation and ozone depletion. Phys Rev Lett 87:78501-1–78501-4. https://doi.org/10.1103/physrevlett.87.078501

Martin F, Burrow PD, Cai Z et al (2004) DNA strand breaks induced by 0–4 eV electrons: the role of shape resonances. Phys Rev Lett 93:68101. https://doi.org/10.1103/physrevlett.93.068101

McNamara A, Geng C, Turner R et al (2017) Validation of the radiobiology toolkit TOPAS-nBio in simple DNA geometries. Phys Med 33:207–215. https://doi.org/10.1016/j.ejmp.2016.12.010
McNaught AD (1997) Compendium of chemical terminology. Blackwell Science, Oxford
Meesungnoen J, Jay-Gerin J-P, Filali-Mouhim A, Mankhetkorn S (2002) Low-energy electron penetration range in liquid water. Radiat Res 158:657–660. https://doi.org/10.1667/0033-7587(2002)158%5b0657:leepri%5d2.0.co;2
Meesungnoen J, Filali-Mouhim A, Ayudhya NSN et al (2003) Multiple ionization effects on the yields of HO2./O2.-and H2O2 produced in the radiolysis of liquid water with high-LET12C6+ ions: a Monte-Carlo simulation study. Chem Phys Lett 377:419–425. https://doi.org/10.1016/s0009-2614(03)01101-1
Meesungnoen J, Sanguanmith S, Jay-Gerin JP (2015) Yields of H_2 and hydrated electrons in low-LET radiolysis of water determined by Monte Carlo track chemistry simulations using phenol/N2O aqueous solutions up to 350 °C. RSC Adv 5:76813–76824. https://doi.org/10.1039/c5ra15801j
Michaud M, Sanche L (1984a) Interaction of low-energy electrons (1–30 eV) with condensed molecules: II. Vibrational-librational excitation and shape resonances in thin N_2 and CO films. Phys Rev B 30:6078
Michaud M, Sanche L (1984b) Interaction of low-energy electrons (1–30 eV) with condensed molecules: I. Multiple scattering theory. Phys Rev B 30:6067–6077
Michaud M, Sanche L (1987a) Absolute vibrational excitation cross sections for slow-electron (1 > 18 eV) scattering in solid H_2O. Phys Rev A 36:4684–4699. https://doi.org/10.1103/physreva.36.4684
Michaud M, Sanche L (1987b) Total cross sections for slow-electron (1–20 eV) scattering in solid H_2O. Phys Rev A 36:4672–4683. https://doi.org/10.1103/physreva.36.4672
Michaud M, Sanche L (1994) Low-energy electron-energy-loss spectroscopy of solid films of argon: surface and bulk valence excitons. Phys Rev B 50:4725–4732
Michaud M, Cloutier P, Sanche L (1991) Phonon excitations in low-energy-electron scattering from solid Ar, Kr, and Xe films: direct observation of conduction-band density of states. Phys Rev B 44:10485
Michaud M, Wen A, Sanche L (2003) Cross sections for low-energy (1–100 eV) electron elastic and inelastic scattering in amorphous ice. Radiat Res 159:3–22. https://doi.org/10.1667/0033-7587(2003)159%5b0003:csflee%5d2.0.co;2
Michaud M, Bazin M, Sanche L (2012) Absolute cross sections for vibrational excitations of cytosine by low energy electron impact. J Chem Phys 137:115103. https://doi.org/10.1063/1.4752655
Michaud M, Bazin M, Sanche L (2013) Nanodosimetry of Auger electrons: a case study from the decay of 125 I and 0–18-eV electron stopping cross sections of cytosine. Phys Rev E 87:32701. https://doi.org/10.1103/physreve.87.032701
Mucke M, Braune M, Barth S et al (2010) A hitherto unrecognized source of low-energy electrons in water. Nat Phys 6:143–146. https://doi.org/10.1038/nphys1500
Muñoz A, Blanco F, Garcia G et al (2008) Single electron tracks in water vapour for energies below 100 eV. Int J Mass Spectrom 277:175–179. https://doi.org/10.1016/j.ijms.2008.04.028
Nagesha K, Sanche L (1998) Effects of band structure on electron attachment to adsorbed molecules: cross section enhancements via coupling to image states. Phys Rev Lett 81:5892–5895. https://doi.org/10.1103/physrevlett.81.5892
Nenner I, Schulz GJ (1975) Temporary negative ions and electron affinities of benzene and N-heterocyclic molecules: pyridine, pyridazine, pyrimidine, pyrazine, and s-triazine. J Chem Phys 62:1747–1758. https://doi.org/10.1063/1.430700
Nikjoo H, Lindborg L (2010) RBE of low energy electrons and photons. Phys Med Biol 55:R65–R109. https://doi.org/10.1088/0031-9155/55/10/r01
Nikjoo H, Uehara S, Emfietzoglou D, Cucinotta FA (2006) Track-structure codes in radiation research. Radiat Meas 41:1052–1074. https://doi.org/10.1016/j.radmeas.2006.02.001
Nikjoo H, Emfietzoglou D, Liamsuwan T et al (2016) Radiation track, DNA damage and response—a review. Rep Prog Phys 79. https://doi.org/10.1088/0034-4885/79/11/116601

Norbury JW, Schimmerling W, Slaba TC et al (2016) Galactic cosmic ray simulation at the NASA Space Radiation Laboratory. Life Sci Sp Res 8:38–51. https://doi.org/10.1016/j.lssr.2016.02.001
Pan X, Sanche L (2006) Dissociative electron attachment to DNA basic constituents: the phosphate group. Chem Phys Lett 421:404–408. https://doi.org/10.1016/j.cplett.2006.01.099
Panajotović R, Michaud M, Sanche L (2007) Cross sections for low-energy electron scattering from adenine in the condensed phase. Phys Chem Chem Phys 9:138–148. https://doi.org/10.1039/b612700b
Park YS, Cho H, Parenteau L et al (2006) Cross sections for electron trapping by DNA and its component subunits I: Condensed tetrahydrofuran deposited on Kr. J Chem Phys 125:74714. https://doi.org/10.1063/1.2229201
Pater P, Seuntjens J, El Naqa I, Bernal MA (2014) On the consistency of Monte Carlo track structure DNA damage simulations. Med Phys 41:121708. https://doi.org/10.1118/1.4901555
Pimblott SM, LaVerne JA (2007) Production of low-energy electrons by ionizing radiation. Radiat Phys Chem 76:1244–1247. https://doi.org/10.1016/j.radphyschem.2007.02.012
Pimblott SM, Laverne JA, Mozumder A (1996) Monte Carlo simulation of range and energy deposition by electrons in gaseous and liquid water. J Phys Chem 100:8595–8606
Plante I (2011) A Monte-Carlo step-by-step simulation code of the non-homogeneous chemistry of the radiolysis of water and aqueous solutions-Part II: Calculation of radiolytic yields under different conditions of LET, pH, and temperature. Radiat Environ Biophys 50:405–415. https://doi.org/10.1007/s00411-011-0368-7
Plante I, Cucinotta FA (2009) Cross sections for the interactions of 1 eV–100 MeV electrons in liquid water and application to Monte-Carlo simulation of HZE radiation tracks. New J Phys 11:63047. https://doi.org/10.1088/1367-2630/11/6/063047
Plante I, Tippayamontri T, Autsavapromporn N et al (2012) Monte Carlo simulation of the radiolysis of the ceric sulfate dosimeter by low linear energy transfer radiation. Can J Chem 90:717–723. https://doi.org/10.1139/v2012-052
Ptasinska S, Denifl S, Abedi A et al (2003) Dissociative electron attachment to gas-phase glycine. Anal Bioanal Chem 377:1115–1119. https://doi.org/10.1007/s00216-003-2254-x
Rackwitz J, Kopyra J, Dąbkowska I et al (2016) Sensitizing DNA towards low-energy electrons with 2-fluoroadenine. Angew Chemie Int Ed 55:10248–10252. https://doi.org/10.1002/anie.201603464
Rackwitz J, Ranković ML, Milosavljević AR, Bald I (2017) A novel setup for the determination of absolute cross sections for low-energy electron induced strand breaks in oligonucleotides—the effect of the radiosensitizer 5-fluorouracil*. Eur Phys J D 71:32. https://doi.org/10.1140/epjd/e2016-70608-4
Rahman WN, Bishara N, Ackerly T et al (2009) Enhancement of radiation effects by gold nanoparticles for superficial radiation therapy. Nanomed Nanotechnol Biol Med 5:136–142. https://doi.org/10.1016/j.nano.2009.01.014
Reilly RM (2008) Biopharmaceuticals as targeting vehicles for in situ radiotherapy of malignancies. In: Modern biopharmaceuticals. Wiley-Blackwell, pp 497–535
Rezaee M, Cloutier P, Bass AD et al (2012) Absolute cross section for low-energy-electron damage to condensed macromolecules: a case study of DNA. Phys Rev E 86:31913. https://doi.org/10.1103/physreve.86.031913
Rezaee M, Hunting DJ, Sanche L (2014) Correlation between energy deposition and molecular damage from Auger electrons: a case study of ultra-low energy (5–18 eV) electron interactions with DNA. Med Phys 41:72502. https://doi.org/10.1118/1.4881329
Rezaee M, Hill RP, Jaffray DA (2017) The exploitation of low-energy electrons in cancer treatment. Radiat Res 188:123–143. https://doi.org/10.1667/rr14727.1
Rogers DWO (2006) Fifty years of Monte Carlo simulations for medical physics. Phys Med Biol 51:R287–R301. https://doi.org/10.1088/0031-9155/51/13/r17
Samara M, Michell RG, Redmon RJ (2015) Low-altitude satellite measurements of pulsating auroral electrons. J Geophys Res A Sp Phys 120:8111–8124. https://doi.org/10.1002/2015ja021292

Sanche L (2010) Low-energy electron interaction with DNA: bond dissociation and formation of transient anions, radicals, and radicals anions. In: Greenberg MM (ed) Radical and radical ion reactivity in nucleic acid chemistry, John Wiley. Wiley, Inc, pp 239–294

Sanche L (2015) Cancer treatment: Low-energy electron therapy. Nat Mater 14:861–863. https://doi.org/10.1038/nmat4333

Sanche L, Schulz GJ (1972) Electron transmission spectroscopy: core-excited resonances in diatomic molecules. Phys Rev A 6:69

Sanz AG, Fuss MC, Muñoz A et al (2012) Modelling low energy electron and positron tracks for biomedical applications. Int J Radiat Biol 88:71–76. https://doi.org/10.3109/09553002.2011.624151

Scheer AM, Mozejko P, Gallup GA, Burrow PD (2007) Total dissociative electron attachment cross sections of selected amino acids. J Chem Phys 126:174301. https://doi.org/10.1063/1.2727460

Schulz GJ (1973) Resonances in electon impact on diatomic molecules. Rev Mod Phys 45:423

Schulz GJ (1976) Principles of Laser Plasmas. Ed G Bekefi, J Wiley Adson 33

Schürmann R, Tsering T, Tanzer K et al (2017) Resonant formation of strand breaks in sensitized oligonucleotides induced by low-energy electrons (0.5–9 eV). Angew Chemie Int Ed 56:10952–10955. https://doi.org/10.1002/anie.201705504

Seiwert TY, Salama JK, Vokes EE (2007) The concurrent chemoradiation paradigm—general principles. Nat Clin Pract Oncol 4:86–100. https://doi.org/10.1038/ncponc0714

Seng G, Linder F (1976) Vibrational excitation of polar molecules by electron impact II. Direct and resonant excitation in H_2O. J Phys B Atom Molec Phys 9:2539–2551

Shao Y, Dong Y, Hunting D et al (2017) Unified mechanism for the generation of isolated and clustered DNA damages by a single low energy (5–10 eV) electron. J Phys Chem C 121:2466–2472. https://doi.org/10.1021/acs.jpcc.6b12110

Shea RC, Petzold CJ, Liu J, Kenttämaa HI (2007) Experimental investigations of the internal energy of molecules evaporated via laser-induced acoustic desorption into a Fourier transform ion cyclotron resonance mass spectrometer. Anal Chem 79:1825–1832. https://doi.org/10.1021/ac061596x

Shyn TW, Cho SY, Cravens TE (1988) Vibrational-excitation cross sections of water molecules by electron impact. Phys Rev A 38:678–682. https://doi.org/10.1103/physreva.38.678

Siragusa M, Baiocco G, Fredericia PM et al (2017) The COOLER code: a novel analytical approach to calculate subcellular energy deposition by internal electron emitters. Radiat Res 188:204–220. https://doi.org/10.1667/rr14683.1

Slaba TC, Blattnig SR, Norbury JW et al (2016) Reference field specification and preliminary beam selection strategy for accelerator-based GCR simulation. Life Sci Sp Res 8:52–67. https://doi.org/10.1016/j.lssr.2016.01.001

Smyth M, Kohanoff J (2011) Excess electron localization in solvated DNA bases. Phys Rev Lett 106:238108. https://doi.org/10.1103/physrevlett.106.238108

Smyth M, Kohanoff J, Fabrikant II (2014) Electron-induced hydrogen loss in uracil in a water cluster environment. J Chem Phys 140:184313. https://doi.org/10.1063/1.4874841

Sridharan DM, Chappell LJ, Whalen MK et al (2015) Defining the biological effectiveness of components of high-LET track structure. Radiat Res 184:105–119. https://doi.org/10.1667/rr13684.1

Sulzer P, Ptasinska S, Zappa F et al (2006) Dissociative electron attachment to furan, tetrahydrofuran, and fructose. J Chem Phys 125:44304. https://doi.org/10.1063/1.2222370

Tonzani S, Greene CH (2006) Radiation damage to DNA: electron scattering from the backbone subunits. J Chem Phys 125:94504. https://doi.org/10.1063/1.2333455

Trevisan CS, Orel AE, Rescigno TN (2006) Elastic scattering of low-energy electrons by tetrahydrofuran. J Phys B: At Mol Opt Phys 39:L255–L260. https://doi.org/10.1088/0953-4075/39/12/l01

Uehara S, Nikjoo H (2006) Monte Carlo simulation of water radiolysis for low-energy charged particles. J Radiat Res 47:69–81. https://doi.org/10.1269/jrr.47.69

Vilar MR, Do Rego AMB, Ferraria AM et al (2008) Interaction of self-assembled monolayers of DNA with electrons: HREELS and XPS studies. J Phys Chem B 112:6957–6964. https://doi.org/10.1021/jp8008207

Vinodkumar M, Joshipura KN, Limbachiya C, Mason N (2006) Theoretical calculations of the total and ionization cross sections for electron impact on some simple biomolecules. Phys Rev A 74:22721. https://doi.org/10.1103/physreva.74.022721

Winstead C, McKoy V (2006) Low-energy electron scattering by deoxyribose and related molecules. J Chem Phys 125:74302. https://doi.org/10.1063/1.2263824

Winstead C, McKoy V (2008) Interaction of slow electrons with methyl phosphate esters. Int J Mass Spectrom 277:279–283. https://doi.org/10.1016/j.ijms.2008.04.015

Wu C, Makiuchi Y, Chen C (2010) High-energy electron beam lithography for nanoscale fabrication. Lithography. https://doi.org/10.5772/45639

Zalustky MR (2013) Radionuclide therapy. In: Vertes A, Nagy S, Klencsar Z et al (eds) Handbook of nuclear chemistry. Springer, Heidelberg, pp 2179–2203

Zecca A, Perazzolli C, Brunger MJ (2005) Positron and electron scattering from tetrahydrofuran. J Phys B: At Mol Opt Phys 38:2079–2086. https://doi.org/10.1088/0953-4075/38/13/002

Zeitlin C, Hassler DM, Cucinotta FA et al (2013) Measurements of energetic particle radiation in transit to Mars on the Mars Science Laboratory. Science (80–) 340:1080–1084. https://doi.org/10.1126/science.1235989

Zheng Y, Wagner JR, Sanche L (2006) DNA damage induced by low-energy electrons: electron transfer and diffraction. Phys Rev Lett 96:208101. https://doi.org/10.1103/physrevlett.96.208101